Meteoritics & Planetary Science 36, 135–154 (2001)
Available online at http://www.uark.edu/meteor

The metallographic cooling rate method revised: Application to iron meteorites and mesosiderites

W. D. HOPFE* AND J. I. GOLDSTEIN

College of Engineering, University of Massachusetts, Amherst, Massachusetts 01003, USA
*Correspondence author's e-mail address: hopfe@ecs.umass.edu

(Received 2000 March 14; accepted in revised form 2000 September 29)
(Presented at a special session on the thermal history of meteorites, Johannesburg, South Africa, 1999 July 16)

Abstract–A major revision of the current Saikumar and Goldstein (1988) cooling rate computer model for kamacite growth is presented. This revision incorporates a better fit to the $\alpha/\alpha + \gamma$ phase boundary and to the $\gamma/\alpha + \gamma$ phase boundary particularly below the monotectoid temperature of 400 °C. A reevaluation of the latest diffusivities for the Fe-Ni system as a function of Ni and P content and temperature is made, particularly for kamacite diffusivity below the paramagnetic to ferromagnetic transition.

The revised simulation model is applied to several iron meteorites and several mesosiderites. For the mesosiderites we obtain a cooling rate of 0.2 °C/Ma, about 10× higher than the most recent measured cooling rates. The cooling rate curves from the current model do not accurately predict the central nickel content of taenite halfwidths smaller than ~10 μm. This result calls into question the use of conventional kamacite growth models to explain the microstructure of the mesosiderites. Kamacite regions in mesosiderites may have formed by the same process as decomposed duplex plessite in iron meteorites.

INTRODUCTION

The cooling rates of the metal phases in iron, stony-iron and chondritic meteorites have traditionally been measured using the metallographic cooling rate technique first developed by Wood (1964) and Goldstein and Ogilvie (1965a). The measured cooling rates for individual iron meteorites and the mesosiderites have varied over a period of three decades. These variations have caused several investigators to question the usefulness of the metallographic cooling rate method. However, the reasons for many of the changes in cooling rates are due to improvements in the computer models used for simulating kamacite growth in taenite. For example, the effect of P on the nucleation of kamacite has been observed experimentally (Doan and Goldstein, 1972). The resulting Fe-Ni-P phase diagram can be used to specify the nucleation temperature of kamacite without considering the effect of undercooling. Also, the low-temperature portion of the Fe-Ni phase diagram has been measured (Yang *et al.*, 1996) as well as the effect of P, S, C and Co on the phase boundaries of the Fe-Ni phase diagram (Widge and Goldstein, 1977; Romig and Goldstein, 1978, 1980; Ma *et al.*, 1998). Finally, new Fe-Ni diffusion coefficients have been measured, particularly at low temperatures (Dean and Goldstein, 1986). These coefficients are also a function of P content and the Curie temperature. In this paper we outline a major revision to the current Saikumar and Goldstein (1988) computer model for kamacite growth. This revision incorporates the latest Fe-Ni phase diagram (Yang *et al.*, 1996) and a reevaluation of the latest diffusivities for the Fe-Ni system as a function of Ni content and temperature. In addition, major revisions are made to the computer simulation model. In this paper the revised simulation model is applied to several iron meteorites and mesosiderites. The results for the mesosiderites call into question the conventional kamacite growth models for this unique group of meteorites.

A variety of metallographic cooling rate techniques have been used to determine the cooling rates of the metal phases in meteorites and their parent bodies. Each of these techniques depends on the application of a simulation model for the growth of the kamacite (low Ni, bcc) in a matrix of taenite (high Ni, fcc) during cooling in a parent asteroidal body. The major metallographic cooling rate methods are described below.

1. Taenite Profile-Matching Method–The cooling rates of meteorites can be determined by matching the calculated Ni composition profiles in taenite obtained from computer simulations with the Ni profiles measured in meteoritic taenite (Goldstein and Ogilvie, 1965a). Ni composition profiles are measured for a given meteorite by using an electron microprobe analyzer (EPMA) or an analytical electron microscope (AEM).

2. Taenite Central Ni Content Method (Wood Method)–The Ni content in the center of taenite is computed as a function of bulk Ni, bulk P, and taenite size (half width) and plotted *vs.* the half width of the taenite. Ni contents in the center of taenite phases of specific halfwidths are measured for a given meteorite by using an EPMA or AEM. These data are plotted on the same graph as the computer simulated central Ni content *vs.* taenite half width curves. The measured data should fall along one of the computed iso-cooling rate (Wood) curves. A variation of the Wood method was developed by Rasmussen (1981), who measured the local bulk Ni and bulk P contents for each taenite lamella with the electron microprobe. These Ni and P data, rather than the bulk Ni and P composition, were used to calculate iso-cooling rate curves.

3. Kamacite Bandwidth Method–This method was developed by Goldstein and Short (1967) and directly relates the kamacite bandwidth with the cooling rate. It is assumed that the diffusion distance between adjacent kamacite plates is infinite so that the effect of impingement can be neglected.

4. Kamacite Central Ni Content Method–The central Ni content of kamacite *vs.* the kamacite bandwidth is calculated by computer simulation methods for kamacite growth in taenite. A correlation between central kamacite Ni content and kamacite bandwidth is observed for a given cooling rate (Powell, 1969; Haack *et al.*, 1996). Ni contents in the center of kamacite phases of specific halfwidths are measured for a given meteorite by using the EPMA. These data are plotted on the same graph as the computer simulated central Ni content *vs.* kamacite half width curves. The measured data should fall along one of the computed iso-cooling rate curves.

5. Cloudy Zone Method–A correlation between the size of the tetrataenite phase (island phase) of the cloudy zone in the residual taenite and the cooling rate of the meteorite, as determined by one or more of the metallographic cooling rate methods (1–4 above), was observed by Yang *et al.* (1997). The correlation line is dependent, however, on the accuracy of the cooling rate method used to determine the cooling rate for each meteorite.

In the first four metallographic cooling rate methods, the taenite is formed and the general shape of the kamacite and taenite are frozen at temperatures of around 450 °C. In the cloudy zone method, growth of the cloudy zone is frozen at about a temperature of 250 °C. As the method is used however, the cooling rate is calibrated using one of the first four methods, at about 450 °C. All these cooling rate methods depend on an accurate computer simulation of the kamacite growth process. The exsolution of kamacite from taenite and the subsequent growth of kamacite can be calculated by using appropriate mass transport equations. These equations require specific data such as phase diagram solubilities and mass transport coefficients that vary with temperature and composition. The next section discusses revisions which are made to the data and the current computer simulation programs which form the basis for the metallographic cooling rate method.

THE COMPUTER MODEL: REVISIONS

Phase Diagram

The Saikumar and Goldstein (1988) expressions which describe the Fe-Ni binary and Fe-Ni (P saturated) pseudo binary phase diagrams in the current computer models for kamacite growth need to be revised to incorporate new experimental data and new theoretical phase diagram calculations such as the $\alpha/(\alpha + \gamma)$ and $(\alpha + \gamma)/\gamma$ phase boundaries of the iron-rich section of the Fe-Ni phase diagram, Yang *et al.* (1996). Figure 1 shows the Fe-Ni phase diagram of Yang *et al.* (1996). At ~400 °C, the monotectoid reaction $\gamma_1 \rightarrow \alpha + \gamma_2$ occurs. The γ_2 is a high Ni ferromagnetic fcc phase which transforms to ordered FeNi γ'' at lower temperatures. Because of the monotectoid reaction, there will be no γ from ~41 to ~48 wt% Ni in the Ni composition profile. The γ' phase which forms due to the eutectoid reaction at ~350 °C (Fig. 1) is not observed metallographically in meteorites and is therefore not considered in the computer simulation.

The solvus lines for Fe-Ni binary (Yang *et al.*, 1996) and the Fe-Ni (P saturated) pseudo binary (Romig and Goldstein, 1980) phase diagrams were approximated with polynomial fits by regression analysis to high order equations using 100–200 data points for each boundary as shown in Fig. 2. The nomenclature system of Moren and Goldstein (1978) was used for the $\alpha/(\alpha+\gamma)$ and $(\alpha+\gamma)/\gamma$ boundaries. Data used to develop the equation for the binary Fe-Ni $\alpha/(\alpha + \gamma)$ solvus line are taken from Goldstein and Ogilvie (1965b), Romig and Goldstein (1980), Chuang *et al.* (1986), Reuter *et al.* (1989) and Yang *et al.* (1996). Data used to develop the equation for the pseudo binary Fe-Ni (P saturated) $\alpha/(\alpha+\gamma)$ solvus line are taken from Romig and Goldstein (1980) for temperatures from 700 to 400 °C. For temperatures of 300 °C and below, the Fe-Ni (P saturated) $\alpha/(\alpha + \gamma)$ solvus line (AUN) follows the Fe-Ni $\alpha/(\alpha+\gamma)$ solvus line (ALN). The polynomial equations for the solvus lines are of a form:

$$\text{Solvus line (wt\% Ni)} = A + A1 \times T + A2 \times T^2 + A3 \times T^3 + A4 \times T^4 + A5 \times T^5 \quad (1)$$

where T is the temperature in degrees Celsius. The constants of the regressions are listed in Table 1.

The solubility of Ni is less in phosphorus saturated taenite (γ) than in binary Fe-Ni taenite (γ) (Romig and Goldstein, 1980). No data are available for temperatures less than the monotectoid at 400 °C. In this model, we assume that the Ni solubility in the phosphorus saturated ferromagnetic taenite, γ_2 or γ'', which forms below 400 °C, is also less than in the binary γ_2 or γ'' (Fig. 2). We assume that the Ni solubility in ternary (P saturated) γ_2 or γ'', (GUN) follows the same functionality as GLN with temperature and contains 1.0 wt% less Ni at all temperatures.

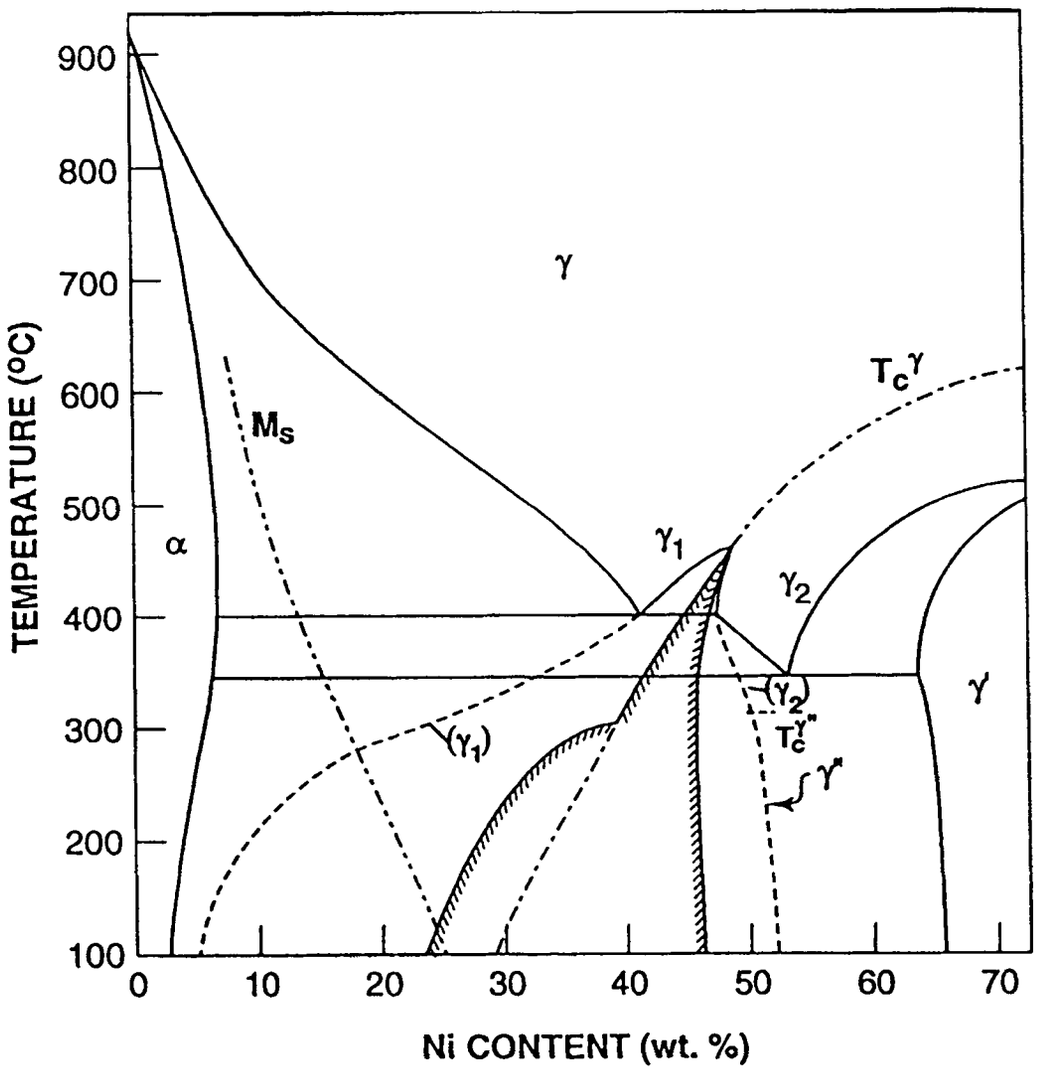

FIG. 1. Fe-Ni phase diagram (Yang *et al.*, 1996). On this diagram, α represents a low-Ni bcc phase, γ represents a high-Ni fcc phase, γ_1 represents a low-Ni paramagnetic fcc phase, γ_2 represents a high-Ni ferromagnetic fcc phase, γ' represents ordered Ni_3Fe, γ'' represents ordered FeNi-tetrataenite, and M_s represents the martensitic transformation starting temperature. $T_c\gamma$ is the Curie temperature of the γ phase. $T_c\gamma''$ is the ordering temperature of FeNi, γ''.

TABLE 1. Constants of polynomial fit.

Solvus line	A	A1	A2	A3	A4	A5
$\alpha/(\alpha+\gamma)$						
ALN (T = 900–100 °C)	0.53671	0.01380	2.64×10^{-5}	-8.58×10^{-8}	4.37×10^{-11}	–
$(\alpha+\gamma)/\gamma$						
GLN (T > 400 °C)	−217.664	1.8957	-4.802×10^{-3}	4.918×10^{-6}	-1.804×10^{-9}	–
$\alpha/(\alpha+\gamma)$ (P saturated)						
AUN (T = 900–100 °C)	19.2462	−0.2686	1.423×10^{-3}	-3.07×10^{-6}	2.92×10^{-9}	-1.02×10^{-12}
$(\alpha+\gamma)/\gamma$ (P saturated)						
GUN (T > 400 °C)	83.887	−0.4406	2.232×10^{-3}	-5.61×10^{-6}	6.07×10^{-9}	-2.34×10^{-12}
$(\alpha+\gamma)/\gamma$						
GLN (T < 400 °C)	38.2130	0.37410	-3.716×10^{-3}	1.712×10^{-5}	-3.736×10^{-8}	3.072×10^{-11}
$(\alpha+\gamma)/\gamma$ (P saturated)						
GUN (T < 400 °C)	GUN was assumed to be the same as GLN (T < 400 °C) less 1 wt%					

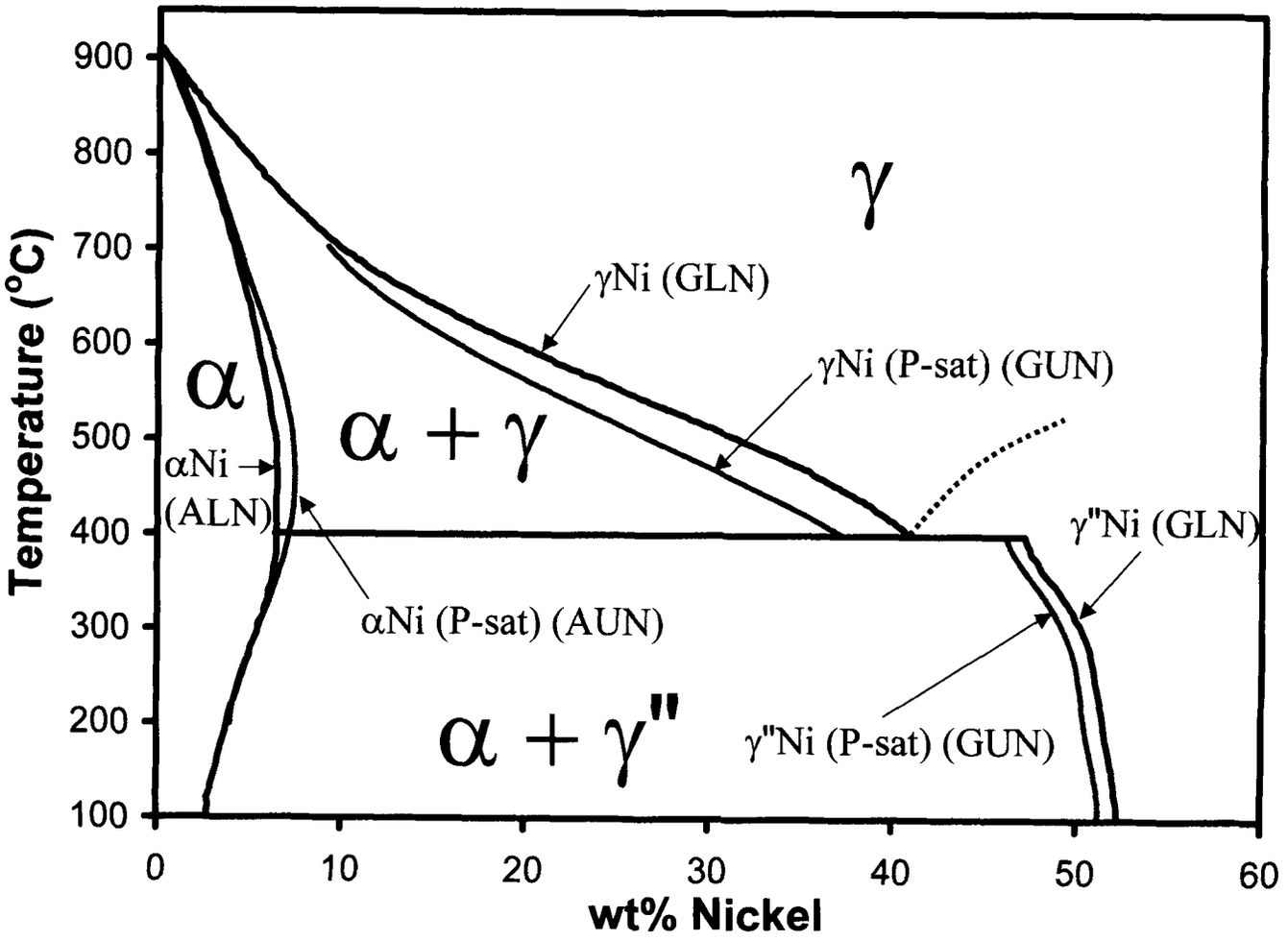

FIG. 2. The binary Fe-Ni and ternary Fe-Ni (P saturated) phase diagrams calculated from the values of ALN, AUN, GLN and GUN (see Table 1 for constants of the solvus lines equations).

The solubility of phosphorus in α kamacite (AUP) and γ taenite (GUP) were determined by Doan and Goldstein (1970) and Romig and Goldstein (1980). Clarke and Goldstein (1978) showed that there is a linear relationship between the logarithm of the P solubility and the inverse of the absolute temperature:

$$\text{AUP (wt\% P)} = \exp(6.3 - 6420.0/T) \quad (2)$$

$$\text{GUP (wt\% P)} = \exp(6.6 - 7800.0/T) \quad (3)$$

where T is the absolute temperature.

The binary Fe-Ni and ternary Fe-Ni (P saturated) phase diagrams calculated from the values of ALN, AUN, GLN and GUN are shown in Fig. 2. A comparison of the calculated ALN and AUN curves with the ALN and AUN curves given by Saikumar and Goldstein (1988) is given in Fig. 3a,b. Pertinent experimental and calculated phase diagram data are also plotted in the figure. The differences between the $\alpha/(\alpha + \gamma)$ solubility curves ALN and AUN are quite significant. Values of the solubility limits above 700 °C and below 300 °C are now consistent with experimental and calculated data. Far more important, the values of ALN are almost 1 wt% higher at kamacite growth temperatures than the values of ALN from Saikumar and Goldstein (1988). Also, the value of AUN at the maximum Ni solubility at about 450 °C is almost 0.5 wt% less than the value of AUN of Saikumar and Goldstein (1988). Incorrect Ni solubility limits in kamacite will give incorrect amounts of kamacite growth and make it impossible to correctly model the Ni content in kamacite (kamacite central Ni content method).

Figure 3c shows a comparison of the new GLN and GUN curves with the GLN and GUN curves given by Saikumar and Goldstein (1988). There are significant differences between these two sets of curves below the monotectoid temperature of 400 °C, particularly GLN. Saikumar and Goldstein (1988) did not fit the binary Fe-Ni $(\alpha + \gamma)/\gamma$ phase boundary (GLN) below the monotectoid temperature, 400 °C. They correctly pointed out that metal in iron meteorites is saturated in P and the interfacial Ni values at growth temperatures below 400 °C are given by the ternary $(\alpha + \gamma)/\gamma$ phase boundary (GUN). The differences between the new GLN and GUN curves and the GLN and GUN curves given by Saikumar and Goldstein (1988) are also due to the assumptions made in the current

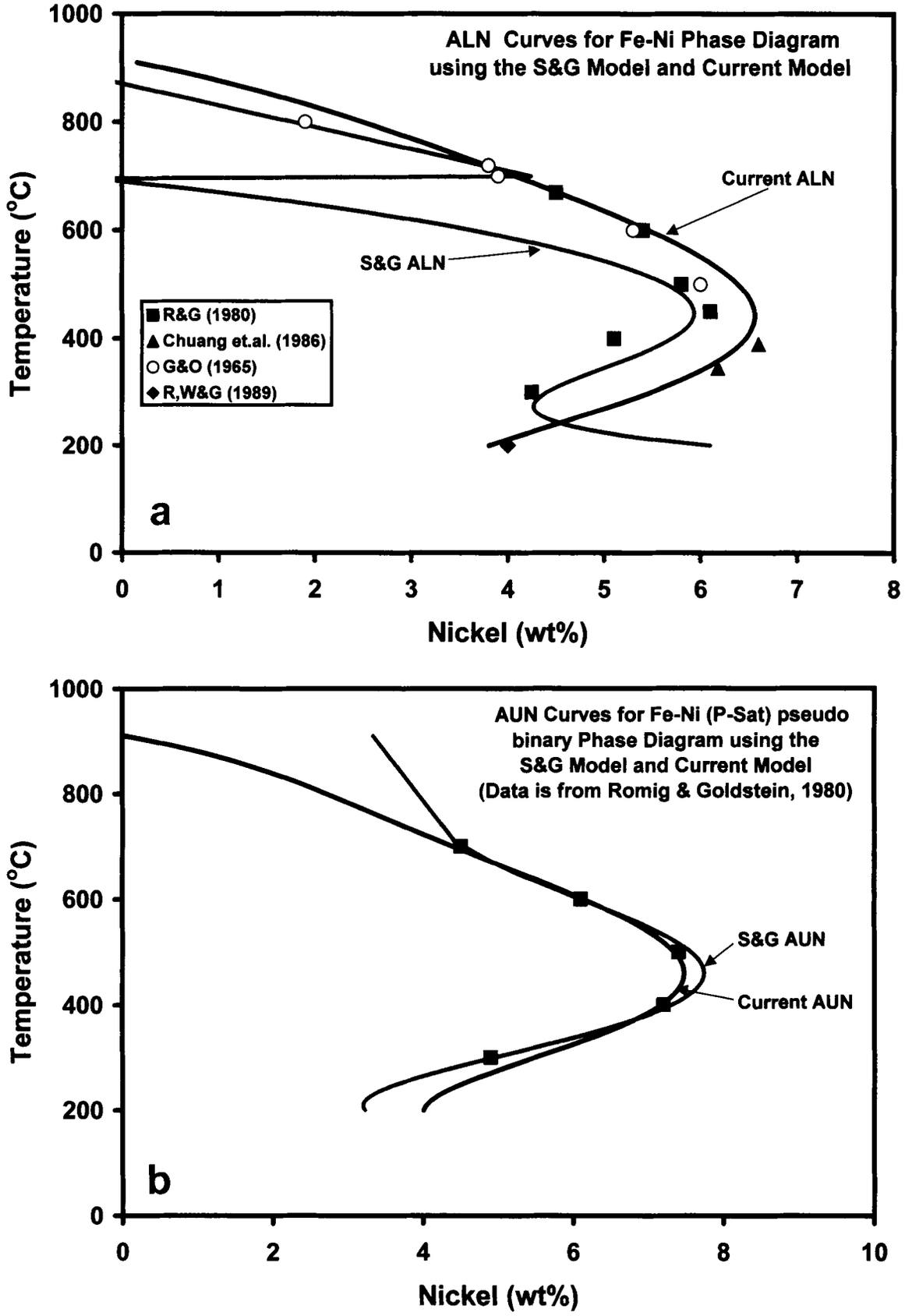

FIG. 3. (a) Comparison of the new ALN curve with that given by Saikumar and Goldstein (1988). Experimental data points are R&G (1980) (from Romig and Goldstein, 1980), Chuang *et al.* (1986), G&O (1965) (from Goldstein and Ogilvie, 1965b), and R,W&G (1989) (from Reuter *et al.*, 1989). (b) Comparison of the new AUN curve with that given by Saikumar and Goldstein (1988). Experimental data points are from Romig and Goldstein (1980). *Figure 3 is continued on the next page.*

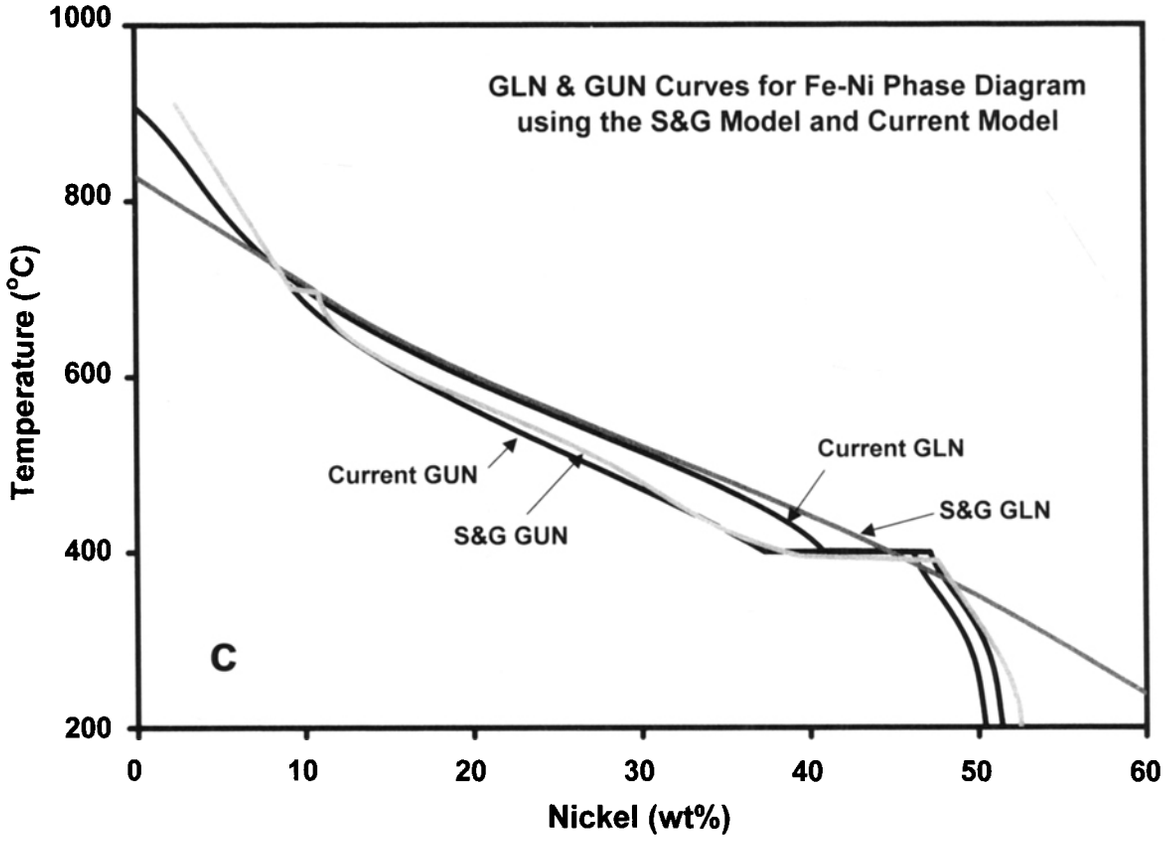

FIG. 3. *Continued.* (c) Comparison of the new GLN and GUN curves with those given by Saikumar and Goldstein (1988). (See Table 1 for constants of the solvus lines equations.)

paper about Ni solubility in γ_2 ,which forms below 400 °C, and in ordered FeNi, γ'', which forms below 310 °C.

The effect of the addition of Co to Fe-Ni alloys is to shift both the $\alpha/(\alpha+\gamma)$ and the $(\alpha+\gamma)/\gamma$ phase boundaries to higher Ni contents at the same temperature or to higher temperatures for the same Ni content (Widge and Goldstein, 1977). Bulk Co contents above 1 wt% are very rare in iron meteorites and the average iron meteorite contains 0.5 wt% (Buchwald, 1975). The effect of Co in iron meteorites is to increase the equilibrium Ni content in taenite by only 0.5 wt% or increase the equilibrium nucleation temperature for kamacite by only about 5 °C. Therefore we can safely assume that the effect of Co on the Fe-Ni (P) pseudo binary which we have modeled above is minimal. Like P, the effect of the addition of Co to Fe-Ni alloys is to aid in the nucleation of kamacite.

The effect of the addition of C to the Fe-Ni alloys is to decrease the Ni content of the $\gamma/(\alpha+\gamma)$ phase boundaries (Romig and Goldstein, 1978). However, since most iron meteorites contain less than 0.01 wt% C (Buchwald, 1975) the effect of C on the Ni content of the $\gamma/(\alpha+\gamma)$ phase boundary is negligible. Even for iron meteorites in groups IAB and IIIE with much higher C contents, most of the C is consumed in the formation of carbides and only small amounts of C remain in solution in the metal phases below 500 °C. Nevertheless, Meibom *et al.* (1994) point out that the effect of C in groups IAB and IIIE may be important in determining accurate cooling rates. The effect of C in the metal phase is assumed to be well within the error limits of the method for the purposes of the present simulation model.

The effect of the addition of S in the Fe-Ni alloys is similar to that of P. The Ni content of the $\alpha/(\alpha+\gamma)$ boundary increases and the Ni content of the $\gamma/(\alpha+\gamma)$ phase boundary decreases (Ma *et al.*, 1998). Since most of the S is consumed in the formation of sulfides, only small amounts of S remain in solution in the metal phases (<0.1 wt%) at 600 °C and below. However, the presence of S does appear to help in the nucleation of the FeNi, γ'' phase (Ma *et al.*, 1998).

Diffusion Coefficients

The current model uses a pseudo-binary approximation for the mass transport equations since the cross coefficients for the ternary system are orders of magnitude less than the main inter-diffusion coefficients (Heyward and Goldstein, 1973). The mass transport equations used for modeling kamacite growth require accurate diffusion coefficients. These mass transport coefficients vary with temperature as well as Ni and P composition. The diffusion coefficients used in the Saikumar and Goldstein (1988) computer model were those of Dean and Goldstein (1986) for Ni in the kamacite (α) and for Ni in the

taenite (γ) in the binary Fe-Ni and the ternary Fe-Ni (saturated P) systems at temperatures below 900 °C.

Saikumar and Goldstein (1988) used the taenite diffusion coefficients of Dean and Goldstein (1986) to fit an expression similar to Goldstein *et al.* (1965) while maintaining the same functional dependence on the nickel content. The equation had the following form:

$$D^{\gamma} = \exp(\mathbf{A} + 0.0519 \times C_{Ni}) \exp\left[\frac{\mathbf{B} + 11.6 \times C_{Ni}}{RT}\right] \quad (4)$$

(where D^{γ} is the interdiffusion coefficient D for Fe-Ni, C_{Ni} is the nickel content in atom percent, T is the temperature in degrees Kelvin and R is the gas constant equal to 1.987 cal/mol K). The constants **A** and **B** were −1.89 and −69 845 cal/mol respectively (Saikumar and Goldstein, 1988).

In the current model the diffusion coefficient for Ni in binary Fe-Ni taenite (γ) was reevaluated using the data of Goldstein *et al.* (1965) and Dean and Goldstein (1986). The data of Goldstein *et al.* (1965) are diffusion coefficients in the γ, that were measured at various nickel contents (10% to 90%) and various temperatures (1000 to 1288 °C). The data of Dean and Goldstein (1986) are diffusion coefficients that were measured at various temperatures between 610 and 925 °C at compositions that were in the single-phase field taenite near the solvus line. A multiple regression was used to fit an equation of the following form:

$$D^{\gamma} = \exp(\mathbf{A} + \mathbf{C} \times (C_{Ni})) \exp\left[\frac{\mathbf{B} + \mathbf{D} \times (C_{Ni})}{RT}\right] \quad (5)$$

where **A, B, C** and **D** are the constants of the regression. The final expression for the diffusion coefficients of Ni in binary taenite is:

$$D^{\gamma} = \exp(1.188 + 0.0185 \times C_{Ni}) \times \exp\left[\frac{-76668 - 116.112 \times C_{Ni}}{RT}\right] \quad (6)$$

The current model had less sum of residuals in fitting the equation to the actual experimental data than the equations that were used in the Saikumar and Goldstein (1988) model. Plots of the calculated diffusion coefficients using the expressions given in this paper and the Saikumar and Goldstein (1988) model along with the experimental data as a function

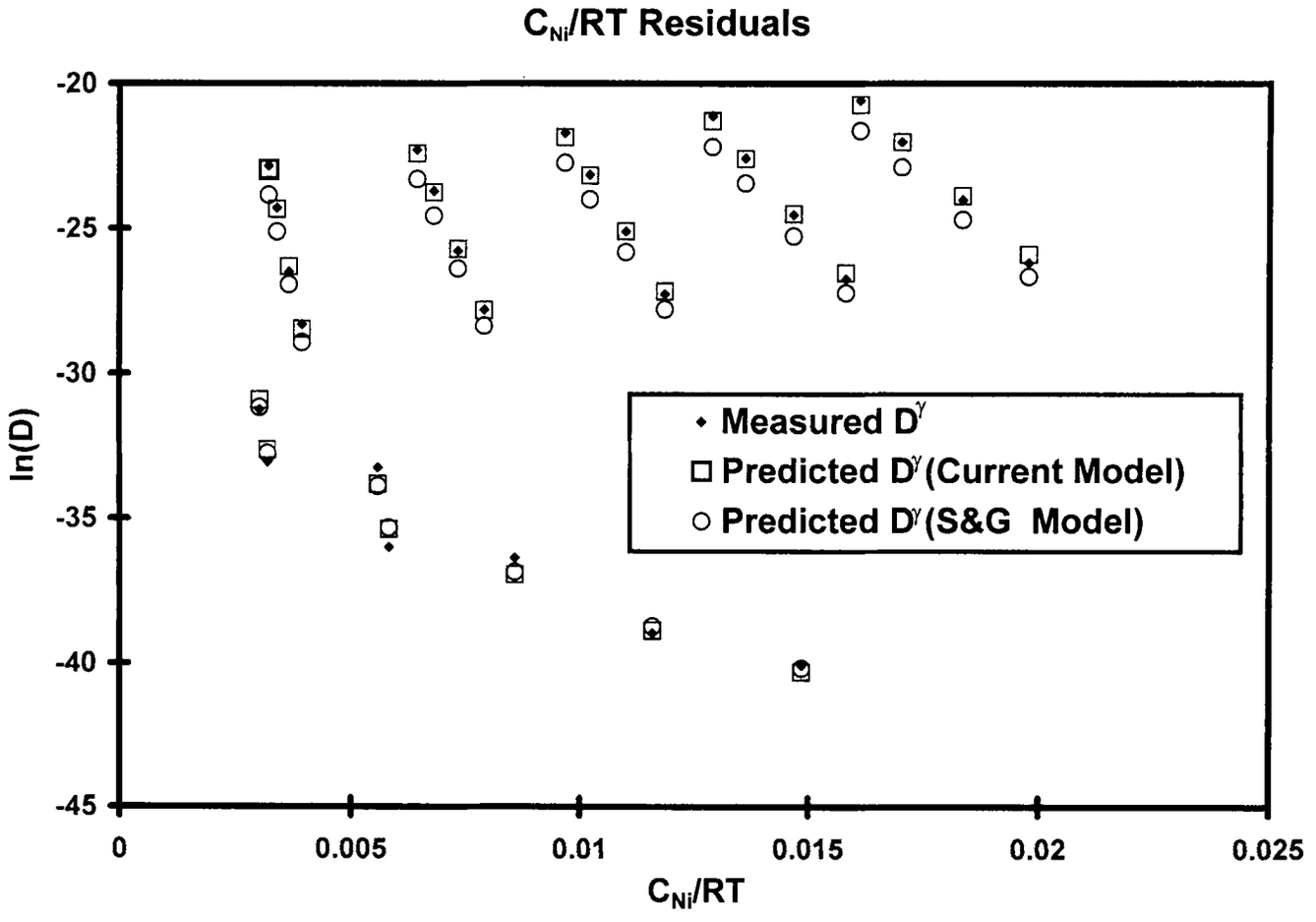

FIG. 4. Comparison of the measured and predicted D^{γ} as a function of the variable C_{Ni}/RT for the current model and the Saikumar and Goldstein (1988) model.

of one of the regression variables, C_{Ni}/RT, is shown in Fig. 4. The calculated diffusion coefficients using the expression given in this paper fit the experimental data much better than the calculated diffusion coefficients from the Saikumar and Goldstein (1988) model. A similar conclusion is reached when plots of calculated and measured diffusion coefficients *vs.* the other regression variables C_{Ni}, and $1/RT$ are compared.

As given by Dean and Goldstein (1986), the ratio of $D^{\gamma}_{\text{ternary}}$ to $D^{\gamma}_{\text{binary}}$ increases as the ratio of the P content in the alloy to the solubility limit of P in the alloy increases. The expression relating $D^{\gamma}_{\text{ternary}}$ to $D^{\gamma}_{\text{binary}}$ can be written as follows:

$$D^{\gamma}_{\text{ternary}} = (1.0 + 9 \times P_{\text{ratio}}) \times D^{\gamma}_{\text{binary}} \tag{7}$$

when the P_{ratio} is <1.

$D^{\gamma}_{\text{ternary}}$ and $D^{\gamma}_{\text{binary}}$ values have been measured to temperatures as low as 610 °C, Dean and Goldstein (1986). Kamacite growth, however, occurs between 650 and 250 °C, a temperature region where values of the controlling diffusivities have not been measured. In the simulation of kamacite growth, we have assumed, as in previous computer models, that the $D^{\gamma}_{\text{ternary}}$ and $D^{\gamma}_{\text{binary}}$ values expressed as a function of T and C_{Ni} can be accurately extrapolated to lower temperatures. This assumption is most likely justified to temperatures above the monotectoid temperature of 400 °C. However, below the monotectoid the taenite phase is metastable γ'' which orders to FeNi, tetrataenite, at 310 °C. In this version of the simulation model we assume that $D^{\gamma}_{\text{binary}}$ and $D^{\gamma}_{\text{ternary}}$ values can be obtained using Eqs. (6) and (7), which were developed for the taenite phase above the monotectoid temperature. The use of these extrapolated diffusivities below 400 °C may lead to errors in the calculation of Ni profiles in taenite above 40 wt% (profile-matching method) or the calculation of Ni contents in the center of taenite (Wood method) for taenite half widths $\leq 10\,\mu$m.

Binary α Fe-Ni alloys are in the paramagnetic state above the Curie temperature of 770 °C. At the Curie temperature, α Fe-Ni changes from paramagnetic state to a ferromagnetic state. Borg and Lai (1963), Hirano *et al.* (1961) and Dean and Goldstein (1986) observed a discontinuity in the slope and value of the diffusivity of Ni from 770 to below 700 °C. Figure 5 shows

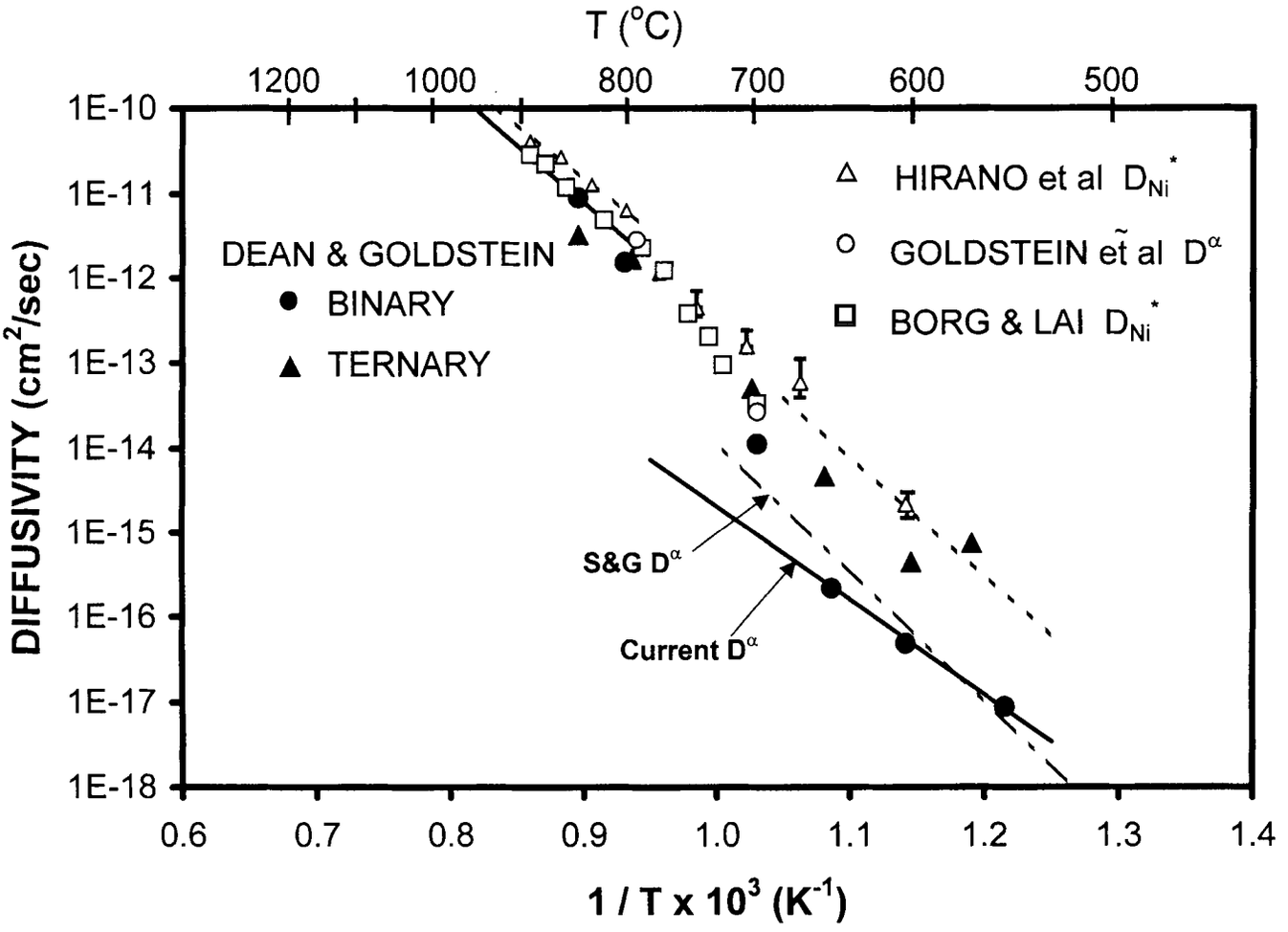

FIG. 5. Comparison of measured binary α-kamacite diffusion coefficients as a function of $1/T$. The line labeled S&G D^{α} represents the fit to D^{α} *vs.* $1/T$ for kamacite from Saikumar and Goldstein (1988) and the line labeled Current D^{α} represents the fit to D^{α} *vs.* $1/T$ obtained from the current study.

the measured diffusivity data. In this study, the diffusion coefficient for Ni in kamacite (α) was reevaluated using the data of Dean and Goldstein (1986). Since the nucleation and growth of the kamacite in meteorites occur at temperatures below 700 °C , only the data below 700 °C were used to fit an Arrhenius type equation $D = D_0\exp(-Q/RT)$ for the diffusion coefficients. It is noted that one of the data points (at 705 °C) of Dean and Goldstein (1986) was ignored in the reevaluation since that data point falls within the temperature range of the paramagnetic to ferromagnetic transition.

The diffusion coefficients for Ni in kamacite (α) in binary Fe-Ni are given by:

$$D^{\alpha} = 2.57 \times 10^{-4} \exp\left[\frac{-50766}{RT}\right] \quad (8)$$

Dean and Goldstein (1986) observed that the diffusivity of Ni in Fe-Ni-P at a given temperature was dependent on the ratio of the P content in the alloy to the solubility limit of P in the alloy at that temperature (P_{ratio}). $D^{\alpha}_{\text{ternary}}$ in kamacite is expressed as a function of $D^{\alpha}_{\text{binary}}$:

$$D^{\alpha}_{\text{ternary}} = (1.0 + 26.5 \times P_{\text{ratio}}) \times D^{\alpha}_{\text{binary}} \quad (9)$$

The above expression is valid for the case when the P_{ratio} is <1.

In addition to P, iron meteorites also contain C and S. The effects of C and S on the diffusivity of Ni below 700 °C have not been studied. However we believe that the effect of C and S is secondary since most of the C and S is consumed in the formation of carbides and sulfides and very small amounts remain in solution in the metal phases below 500 °C.

The errors in the measurement of interdiffusion coefficients are of the order of ±10 to ±20% (Dean and Goldstein, 1986; Goldstein *et al.*, 1965). The largest error obtained by Dean and Goldstein (1986) of ±50 to ±100% was in their lowest temperature taenite diffusion couple, 610 °C. The effect of errors in the measurement of cooling rates is discussed later in this paper using specific meteorites as examples.

Numerical Model

The computer model that was developed in this study is based on the model proposed by Saikumar and Goldstein (1988). The model uses the Murray and Landis (1959) variable grid spacing technique and the Crank–Nicolson (Noye, 1984) approximation for the diffusional growth of kamacite in taenite. The velocity of the interface is determined at each timestep with a Ni mass balance in the taenite and kamacite. The amount of Ni is kept constant in the system. In the Saikumar and Goldstein (1988) model, rod geometries were used in the simulation of the exsolution of kamacite from taenite. In the model developed here, plate morphology was assumed since the Widmanstätten pattern is formed by the growth of kamacite plates in a taenite matrix. The present model assumes that the meteorite's thermal history was linear. Nucleation of kamacite in the Fe-Ni-P containing taenite is assumed to occur at a temperature below that at which phosphides (Ph) are first formed during cooling. The solubility of P in taenite (Eq. (3)) determines the temperature where phosphides form. As shown experimentally (Narayan and Goldstein, 1984a,b), the nucleation of kamacite occurs at the temperature when the meteorite enters the three phase field, $\alpha + \gamma$ + Ph. Rasmussen *et al.* (1995) assumed that kamacite nucleated in the absence of phosphides.

In the Saikumar and Goldstein (1988) model, diffusion in the kamacite phase was assumed to be infinitely fast at temperatures above ~450 °C. This assumption causes problems in modeling the growth of kamacite in iron meteorites with a bulk nickel less than about 7.7 wt%. For example if the bulk Ni content of a meteorite is 7.5 wt%, at about 460 °C during the cooling process, the nickel content of the kamacite at the kamacite/taenite interface is about 7.5 wt%, the bulk Ni content of the meteorite (see Fig. 3a,b). Since the nickel content in the taenite is also above the bulk nickel content in the meteorite, the mass balance of nickel in the kamacite and taenite will cause an excess of nickel to exist in the system and the model can not proceed below 460 °C. In the model developed in this study, kamacite diffusion given by Eq. (9) was incorporated at all growth temperatures. Using this modification, the current model is able to calculate kamacite growth in taenite with a bulk nickel content of less than 7.7 wt% and to calculate Ni gradients in kamacite that may develop at lower temperatures ($T < 500$ °C). It is important to note that most of the numerical models developed before 1988 as summarized by Saikumar and Goldstein (1988) and most models developed after 1988 included the effect of diffusion in kamacite.

In the Saikumar and Goldstein (1988) model the interface between the kamacite and taenite was only allowed to move in one direction, to deplete the taenite phase. In the model developed in this study, the movement of the kamacite/taenite interface was allowed to move in either direction to allow for kamacite regression at lower temperatures.

APPLICATION TO IRON METEORITES

Toluca

Toluca is an iron meteorite of chemical group IA with a bulk composition of ~8.14 wt% Ni and 0.16 wt% P (Buchwald, 1975). Kamacite growth was simulated for several linear cooling rates (cooling from 700 to 200 °C) and a number of impingement lengths to develop appropriate curves using the Wood method. Figure 6a shows the results of a computer simulation of Widmanstätten growth in Toluca for a cooling rate of 25 °C/Ma, an impingement length of 700 μm, and a precipitation temperature of 700 °C. The computer simulation used 200 points, 50 in the kamacite and 150 in the taenite. The calculated Ni concentration profiles which develop at

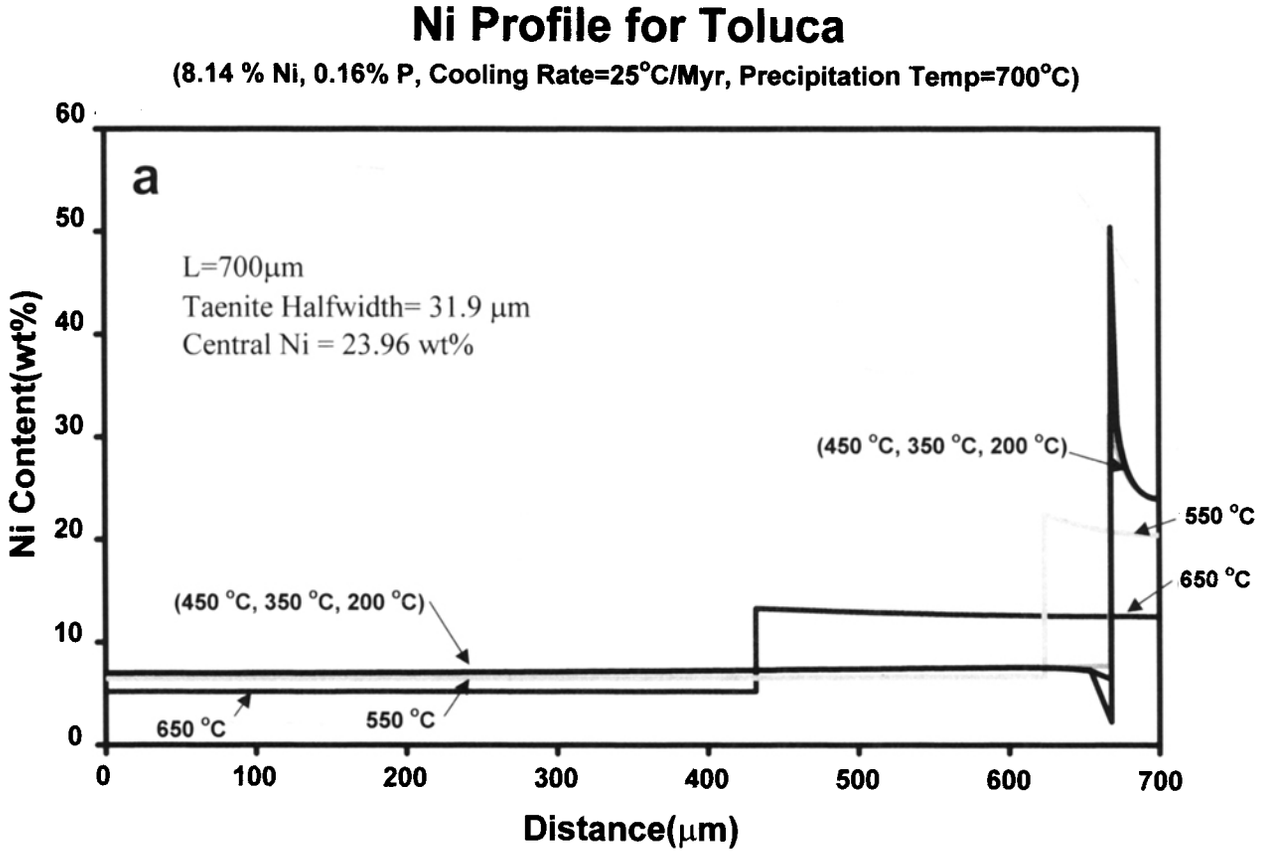

FIG. 6. (a) Nickel concentration profiles as a function of temperature calculated using a computer simulation of Widmanstätten growth in the Toluca iron meteorite (cooling rate = 25 °C/Ma, impingement length = 700 μm, precipitation temperature = 700 °C, final cooling temperature = 200 °C, 200 points were used in the simulation). (facing page, top) (b) Nickel concentration profiles in kamacite and taenite $\pm 20\,\mu$m from the kamacite/taenite boundary at 450, 350 and 200 °C. The Ni profiles are calculated using a computer simulation of Widmanstätten growth in the Toluca iron meteorite. Note that the OTR/CZ discontinuity in γ is shown in the profiles for 350 and 200 °C. (facing page, bottom) (c) Nickel concentration profiles in kamacite using a computer simulation of Widmanstätten growth in the Toluca iron meteorite. Note that the gradients in the Ni profile are obtained at temperatures below 550 °C.

various temperatures are shown in Fig. 6a. A significant M-shaped Ni profile develops in taenite at or below 450 °C as shown in Fig. 6b. The computer simulation for the Ni gradient in the taenite phase below 450 °C contains 150 points allowing for a spatial resolution of 0.2 μm per point. This spatial resolution allows one to make a good comparison between EPMA data collected with a spatial resolution at ~1 μm and the spatial resolution of the computer simulation.

A Ni composition gradient develops in kamacite after cooling of ~150 °C below the nucleation temperature of 700 °C. The Ni gradients are significant at lower temperatures (<450 °C) and the Agrell effect near the kamacite/taenite interface is well developed (See Fig. 6c). For the computer simulation with a cooling rate of 25 °C/Ma shown in Fig. 6, the central nickel content of kamacite and taenite was fixed at 450 °C. On the other hand, the composition of nickel near the kamacite/taenite interface varies continuously to much lower temperatures.

Plots of taenite central Ni *vs.* taenite halfwidth using the experimental data for Toluca of Wood (1964) and Saikumar and Goldstein (1988) are shown in Fig. 7. The Wood curves from the current simulation model for three different cooling rates (25, 50 and 100 °C/Ma) and from the calculated curves from Saikumar and Goldstein (1988) are also shown in Fig. 7. The calculated Wood curves from the current model are a better fit to the experimental EPMA data. Nevertheless, the current model still yields the same cooling rate for Toluca, ~25 °C/Ma, as given from the Saikumar and Goldstein (1988) model. Using the profile-matching method, the data of Saikumar and Goldstein (1988), and the new kamacite growth model, consistent cooling rates between 10 and 30 °C/Ma are obtained.

Figure 8 shows the effect of a worst case scenario if one assumes the largest error in the measurement of taenite interdiffusion coefficients is $\pm 100\%$. Plots of taenite central Ni *vs.* taenite halfwidths for Toluca are calculated for a cooling rate of 50 °C/Ma for errors in D^{γ} as large as 2× or as small as 0.5× the D^{γ} given in Eq. (7). In this example, the experimental data fall on the 50 °C/Ma curve when the calculated diffusivity is 2× the best-fit D^{γ} values. We consider a factor of 2 error in the accuracy of the cooling rate to be the maximum error range for the metallographic method.

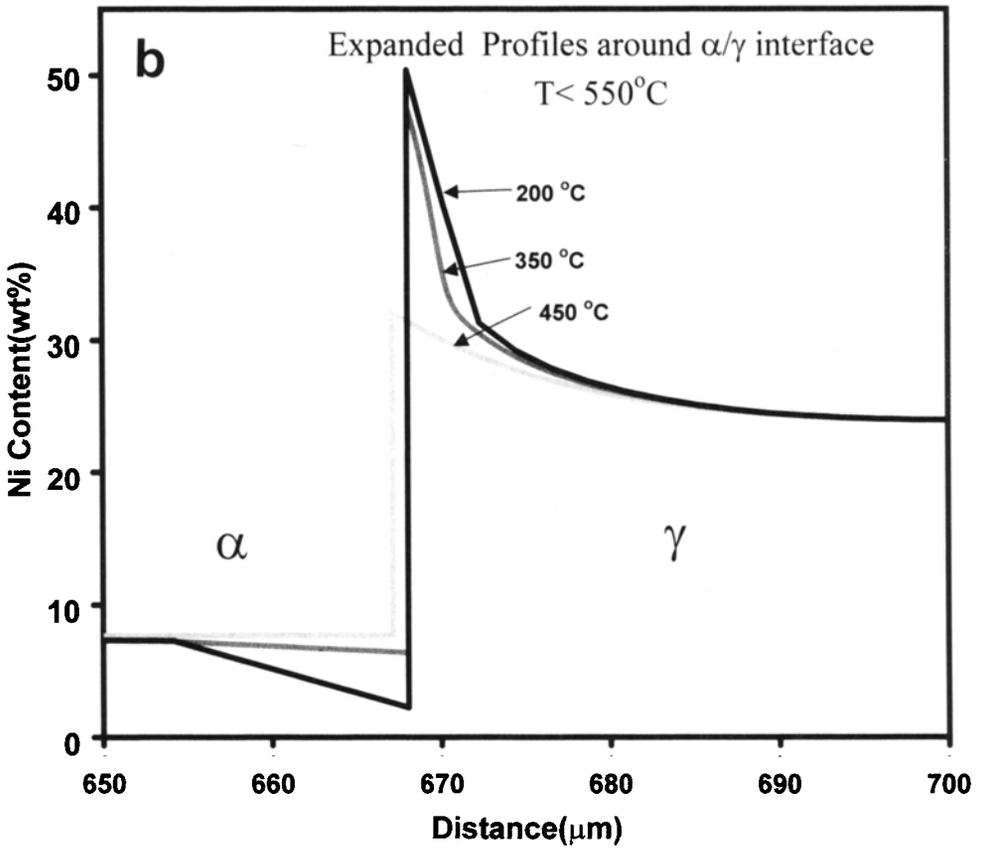

Kamacite Ni Profile for Toluca

(8.14 % Ni, 0.16% P, Cooling Rate=25°C/Myr, Precipitation Temp=700°C)

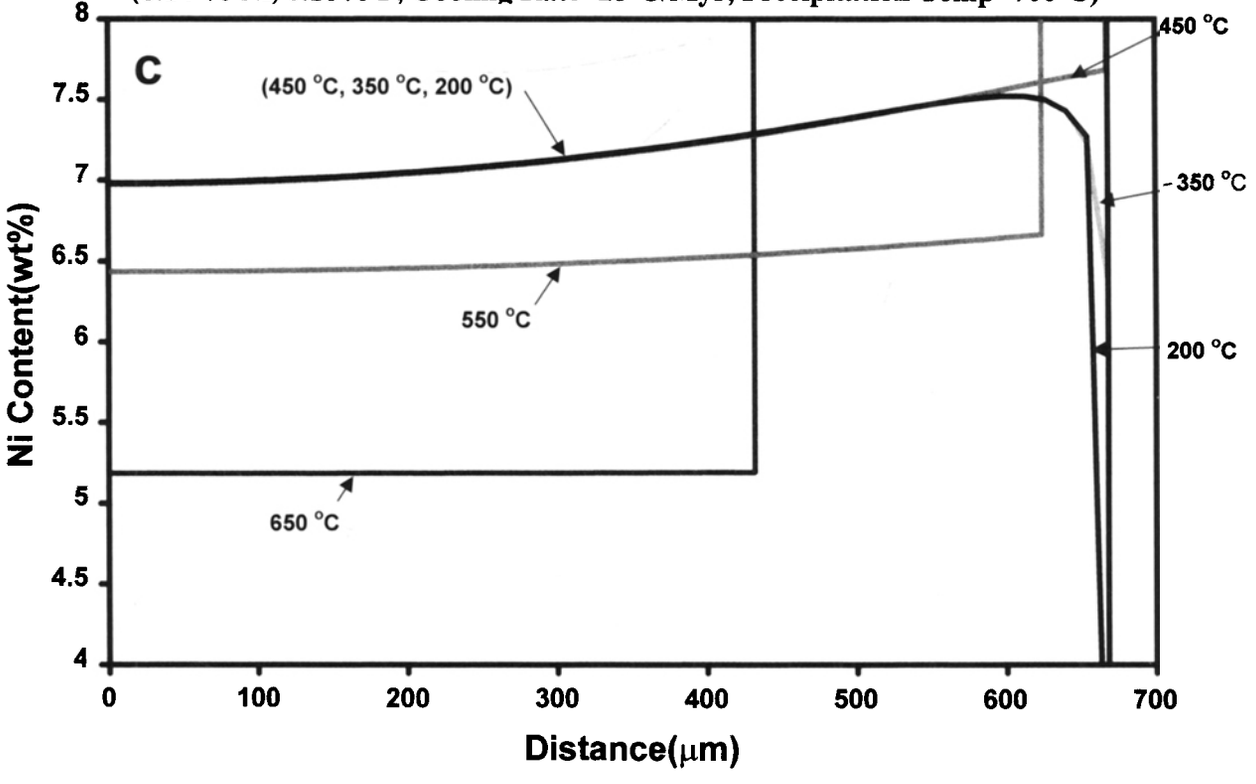

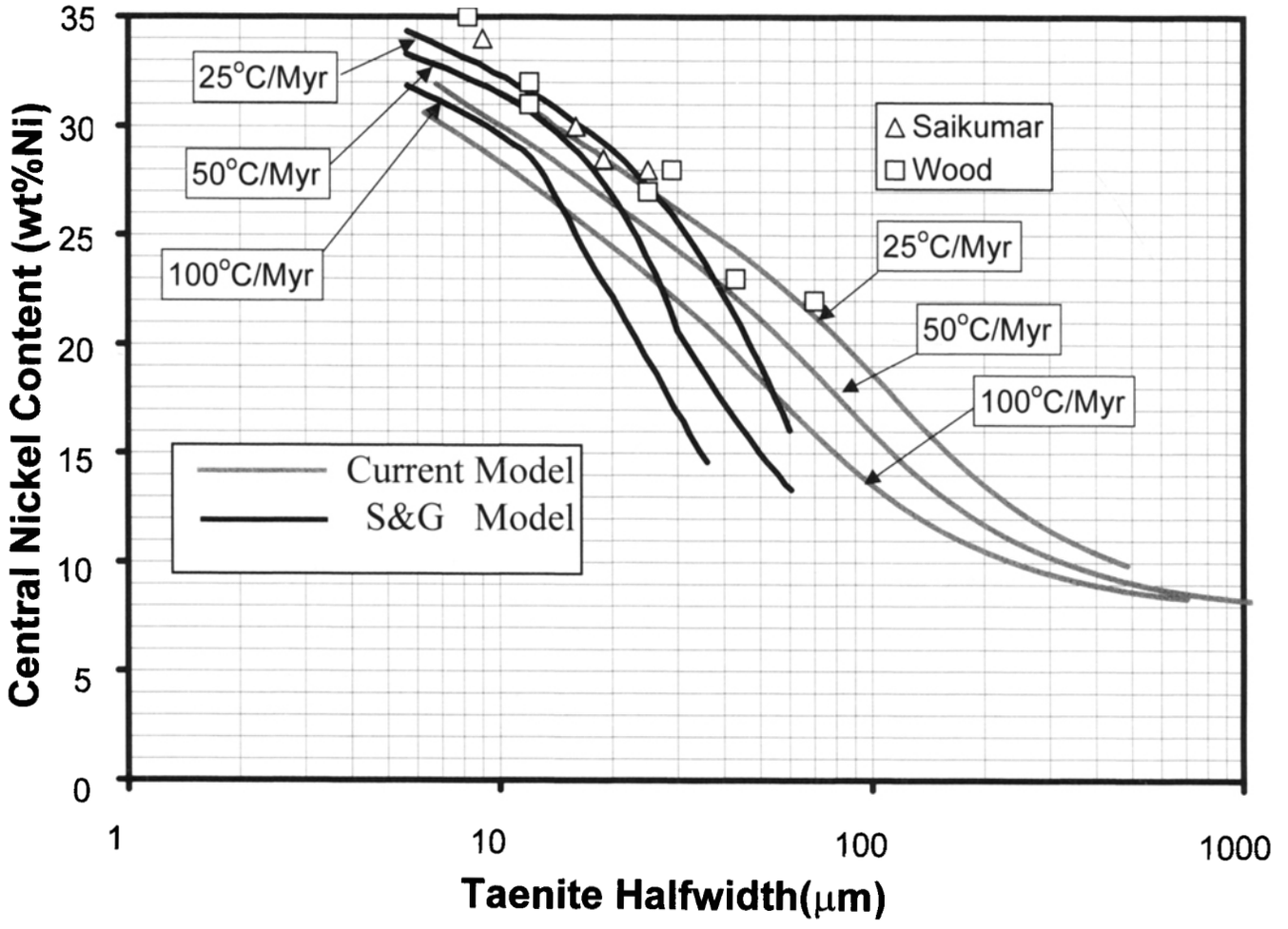

FIG. 7. Cooling rate curves for the Toluca iron meteorite (Wood method) for the current model and for the Saikumar and Goldstein (1988) model. The experimental data are from Saikumar and Goldstein (1988) and Wood (1964).

Canyon Diablo

Canyon Diablo is an iron meteorite of chemical group IAB with a composition of ~7.1 wt% Ni and 0.26 wt% P (Buchwald, 1975). Kamacite growth was simulated for several linear cooling rates (cooling from 700 and 200 °C). Figure 9 shows the results of a computer simulation of Widmanstätten growth in Canyon Diablo for a cooling rate of 100 °C/Ma, an impingement length of 2000 μm, and a precipitation temperature of 700 °C. The computer simulation used 160 points, 80 in the kamacite and 80 in the taenite. The Ni concentration profile in kamacite is given in the inset of Fig. 9.

Figure 10 shows EPMA data taken across a kamacite plate ~2000 μm half width (Goldstein, 1965). The Ni profile was modeled for two cooling rates, 20 and 100 °C/Ma with an impingement length of 2000 μm. The kamacite profile is closely matched using either linear cooling rate particularly if one considers the errors in the EPMA data and the uncertainty in the detailed shape of the $\alpha/(\alpha + \gamma)$ boundary of the Fe-Ni (P saturated) phase diagram (Fig. 3b). Although the kamacite profile-matching method and the kamacite central Ni content method can be used to determine cooling rates, the sensitivity of the method is not sufficient to determine which of the two cooling rates is correct for Canyon Diablo. As discussed in the following section on the mesosiderites, it may not be possible to employ information from the kamacite phase to determine cooling rates.

APPLICATION TO MESOSIDERITES

Mesosiderite cooling rates are the slowest yet determined for all the meteorites (Powell, 1969). Powell (1969) used the Wood method and obtained cooling rates of ~0.1 °C/Ma. Haack *et al.* (1996) applied the Wood method, using the phase diagram information and diffusion coefficients of Saikumar and Goldstein (1988), and obtained cooling rates of ~0.03 °C/Ma. Assuming linear cooling from 700 to 200 °C, any cooling rate <0.1 °C/Ma would require a cooling time greater than the time period that elapsed since metal-silicate mixing occurred, more than 4.47 Ga ago (Powell, 1969; Rubin and Mittlefehldt, 1993).

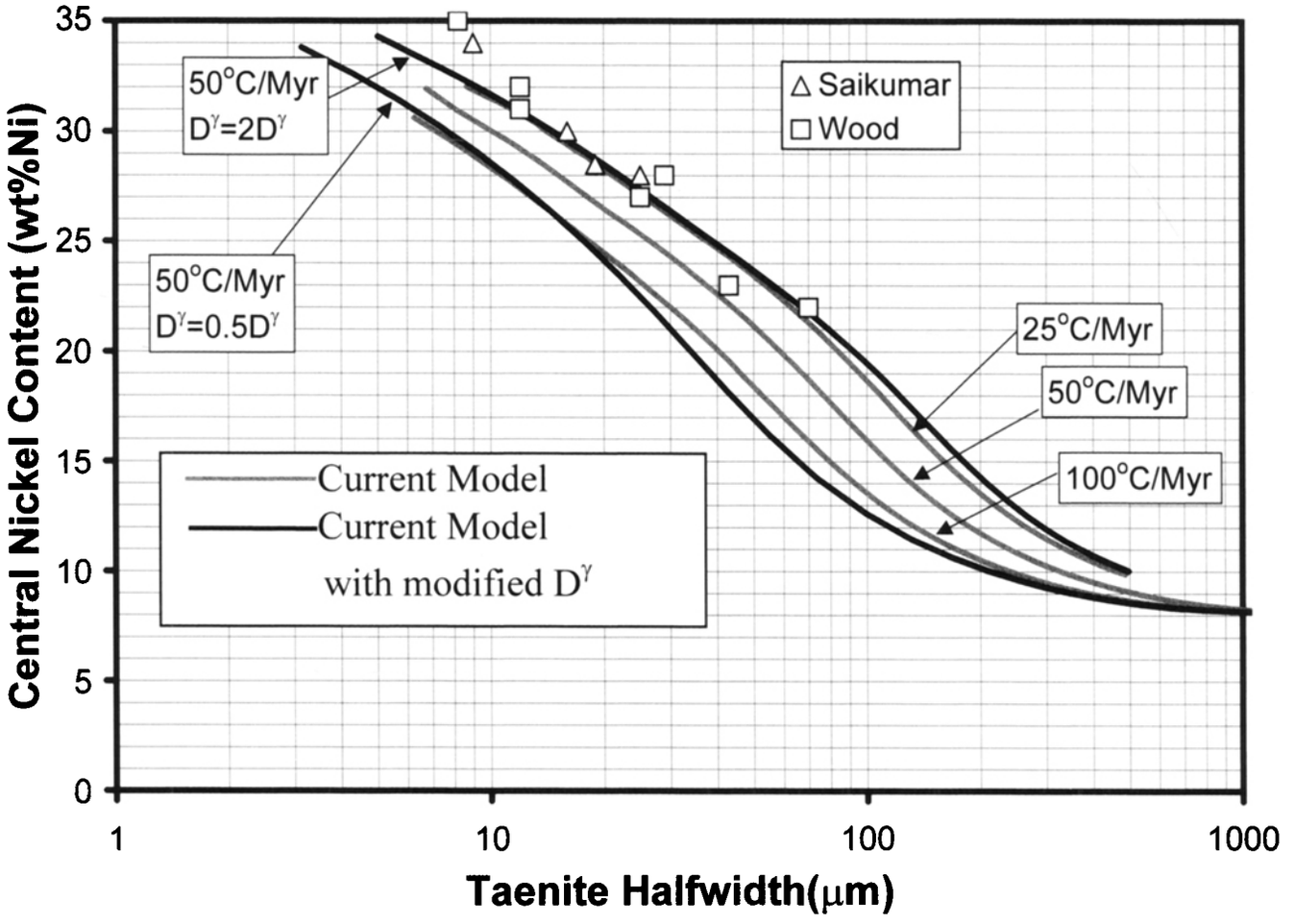

FIG. 8. Cooling rate curves for the Toluca iron meteorite (Wood method) for the current model and for a cooling rate of 50 °C/Ma. The effect of a large error in the measurement of taenite interdiffusion of ±100% on the 50 °C/Ma curve is shown. Errors in D^{γ} are as large as 2× or as small as 0.5× the D^{γ} given in Eq. (7).

Figure 11 shows EPMA data for taenite central Ni content *vs.* taenite half width for four mesosiderites Pinnaroo, Emery, Esterville and Vaca Muerta (Haack *et al.*, 1996). The calculated Wood curves from Haack *et al.* (1996) are also displayed. These curves only consider wide taenite regions with half widths ≥20 μm. According to Haack *et al.* (1996), these curves are not influenced by the monotectic phase transformation which takes place at or below 400 °C. Haack *et al.* (1996) determined a metallographic cooling rate of ~0.03 °C/Ma.

Metallographic cooling rate simulations of taenite central Ni content *vs.* taenite half width were obtained using the kamacite growth model described in this paper for three cooling rates (0.05, 0.1 and 0.5 °C/Ma). The Ni and P contents of 9.78 wt% Ni and 0.15 wt% P were used in the simulation. This Ni content is representative of the four mesosiderites, Pinnaroo, Emery, Esterville and Vaca Muerta, whose Ni contents vary from 7.99 to 10.54 wt% Ni (Hassanzadeh *et al.*, 1990). The cooling rate curves (central taenite Ni *vs.* the total taenite width) for 0.1 and 0.5 °C/Ma are plotted on Fig. 11. The cooling rate curves for the taenite (Fig. 11) fall above the curves of Haack *et al.* (1996). A cooling rate of about 0.2 °C/Ma is predicted using EPMA data for taenite half widths above ~10 μm. This cooling rate is about a factor of 10 higher than that determined by Haack *et al.* (1996). Without access to the Haack *et al.* computer code, we are not sure how our new formulation for the phase diagram or diffusion coefficients may change the Haack *et al.* (1996) calculated Wood curves.

Figure 12 shows a plot of kamacite central Ni *vs.* the kamacite half width for Patwar, Hainholz, Vaca Muerta and Mincy using the EPMA data from Powell (1969). The EPMA measurement errors for the Ni content of individual points is ±0.1 wt% at the 95% confidence limit. The calculated central Ni content *vs.* kamacite half width for cooling rates between 0.001 and 0.1 °C/Ma from Haack *et al.* (1996) are also shown in the figure. The cooling rate curves which enclose the data lie in a range between the 0.001 and the 0.01 °C/Ma. Haack *et al.* (1996) argued that kamacite orientation effects with respect to the polished surface lead to inaccuracies in the measurement of kamacite half width. Any corrections in the measurement of kamacite half widths would move the data closer to the

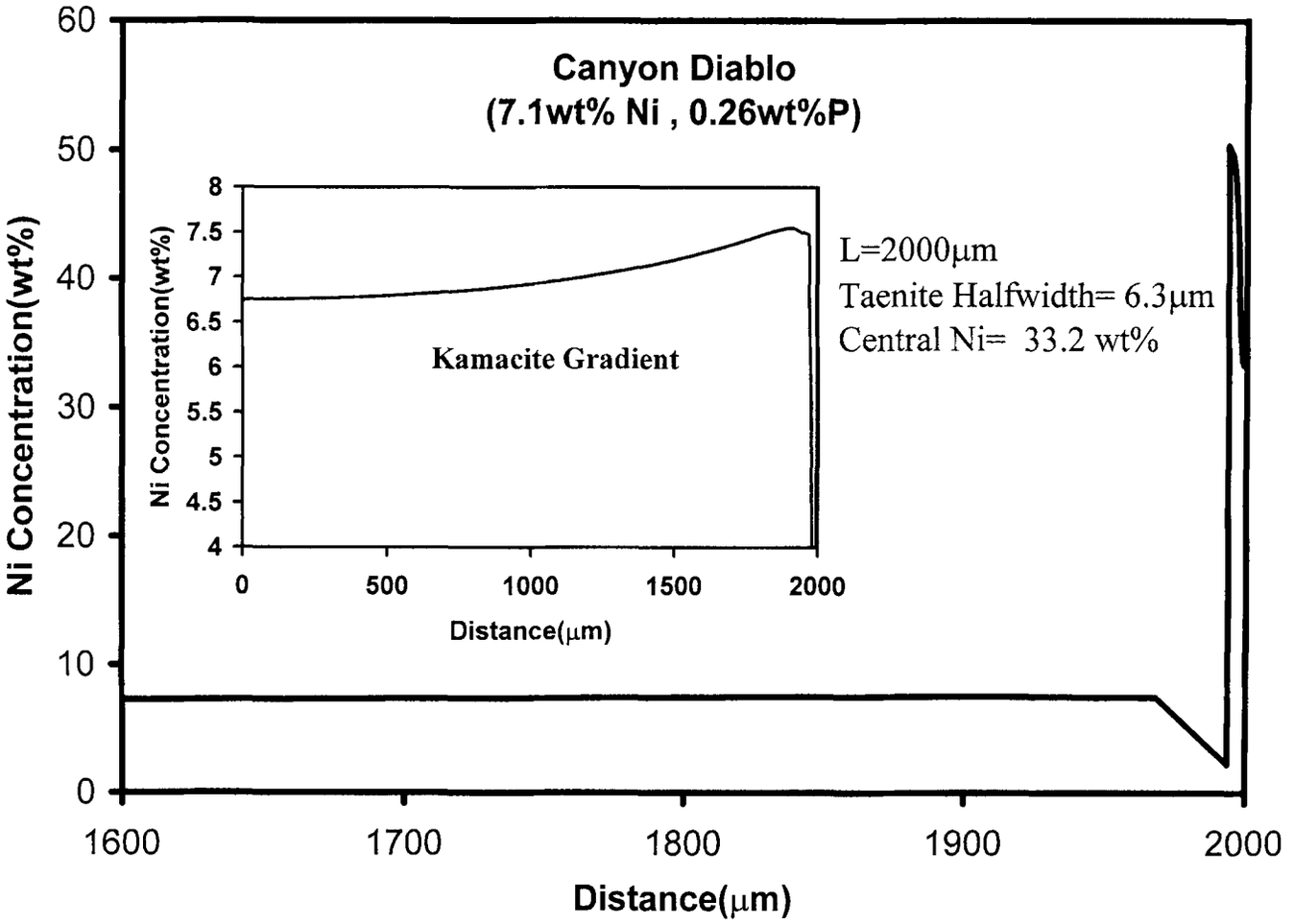

FIG. 9. Nickel concentration profile developed during cooling using a computer simulation of Widmanstätten growth in the Canyon Diablo iron meteorite (cooling rate = 100 °C/Ma, impingement length = 2000 μm, precipitation temperature = 700 °C, final cooling temperature = 200 °C). The larger profile shows the Ni concentration within taenite and ~400 μm of kamacite close to the α/γ boundary. The inset shows the calculated nickel concentration profile in the kamacite.

0.01 °C/Ma curve. However, in two of the four mesosiderites (Vaca Muerta and Patwar) planar kamacite, that formed in a Widmanstätten pattern, was analyzed. Geometric effects should be minimized in these meteorites yet the spread in kamacite Ni data is the same as in the other two mesosiderites (Mincy and Hainholz).

Kamacite cooling rate curves determined from the kamacite growth model described in this paper for 9.78 wt% Ni and 0.15 wt% P are plotted in Fig. 12. The data fall along a cooling rate curve of ~0.05 °C/Ma. The cooling rate curves calculated from the present model also predict much higher cooling rates than the cooling rates of 0.001 to 0.01 °C/Ma of Haack *et al.* (1996).

The computer simulation model correctly predicts that the central Ni content of the kamacite phase increases with increasing size. However, as discussed in the section on iron meteorites, and by Powell (1969) and Haack *et al.* (1996), the uncertainty in the detailed shape of the $\alpha/(\alpha + \gamma)$ solvus line for the Fe-Ni (P saturated) phase diagram, where the Ni contents only vary by a few wt%, can lead to errors in the predicted Ni variation in the kamacite phase as a function of cooling rate. Figure 12 shows that even for one meteorite, that the kamacite Ni content varies by as much as 0.5 wt% for the same-sized kamacite. A variation of 0.5 wt%, however, represents almost an order of magnitude variation in cooling rate. Therefore, the kamacite central Ni content method is relatively insensitive to cooling rate variations and cannot be used to obtain cooling rates for the mesosiderites.

If one assumes an error in the taenite diffusivities of as much a factor of 2 (+100%), we calculate that the cooling rate of the mesosiderites would increase to about 0.4 °C/Ma. The cooling rate of ~0.2 °C/Ma to as high as 0.4 °C/Ma is still a factor of 2.5 to 5 lower than the minimum cooling rate of the 1.0 °C/Ma for the Esterville mesosiderite obtained from independent studies of cation ordering in orthopyroxene crystals (Ganguly *et al.*, 1994).

The faster cooling rates obtained from the taenite central Ni content method *vs.* the kamacite central Ni content method (Figs. 11 and 12) are probably not significant given the inaccuracy of the later method. The taenite central Ni content

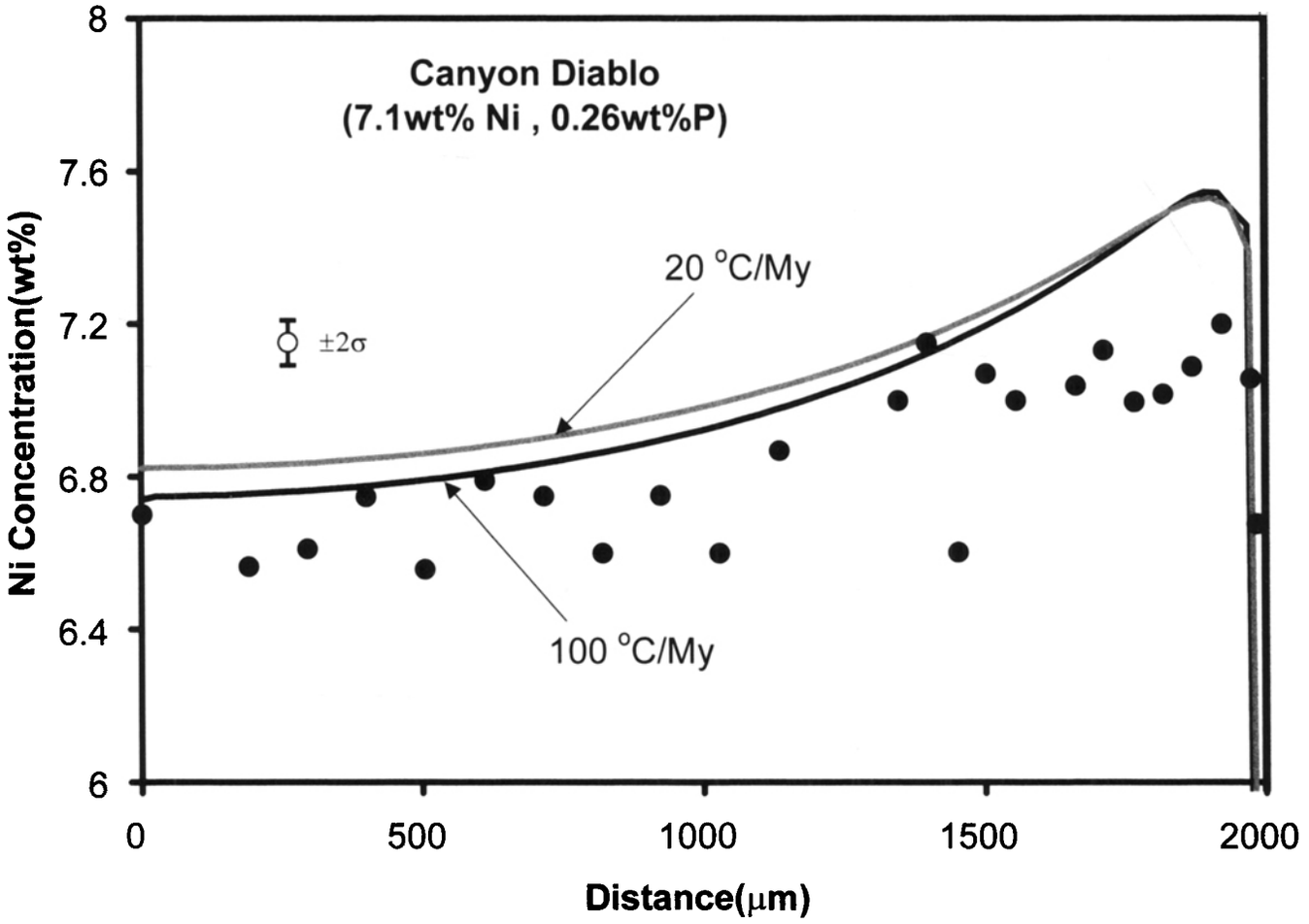

FIG. 10. Nickel concentration *vs.* distance in a kamacite plate, ~2000 μm half width, in the Canyon Diablo iron meteorite as measured using the EPMA (Goldstein, 1965). The Ni profile was also calculated at two cooling rates for the current computer simulation model (cooling rates = 20 and 100 °C/Ma, impingement length = 2000 μm).

method used in this paper, however, predicts cooling rates of about 0.2 °C/Ma for the mesosiderites, a much higher value than that obtained by Haack *et al.* (1996).

Figure 13 shows a measured EPMA Ni composition profile across a kamacite-taenite region from an isolated grain in the Reckling Peak (RKP)A79015 mesosiderite (9.87 wt% Ni, 0.15 wt% P; Jarosewich, 1990). The profile-matching method was used to determine the cooling rate of this meteorite. The match between calculated and measured profiles is not particularly good in part because the model assumes a plate geometry for the kamacite growth. The measured cooling rate is about 0.1 °C/Ma. This cooling rate is within a factor of 2 of the cooling rates of the four mesosiderites (Fig. 11) determined using the kamacite growth model described in this paper.

The cooling rate curves from the current model do not accurately predict the central nickel content of taenite halfwidths smaller than ~10 μm (Fig. 11). There are two possible explanations for this discrepancy:

(1) Diffusion coefficients in the γ'' phase, which forms as a result of the monotectic below 400 °C, may be quite different from D_{binary} and D_{ternary} in the γ phase given by Eqs. (6) and (7). These equations were developed by extrapolating the known diffusivities of the taenite phase above the monotectoid temperature to lower temperatures <400 °C. The γ'' phase and ordered Fe,Ni at lower temperatures have different crystal structures and vacancy concentrations which control the rate of mass transport. The use of extrapolated diffusivities (Eqs. (6) and (7)) may lead to errors in the calculation of Ni profiles in taenite above 40 wt% (profile-matching method) or the calculation of Ni contents in the center of taenite (Wood method) for taenite half widths ≤ 10 μm.

(2) The formation of kamacite in mesosiderites may not occur by the same transformation sequence as for the iron meteorite Widmanstätten pattern (the slow cooling of taenite and the exsolution of kamacite at low temperatures). If the mesosiderites cool fairly rapidly, ~1 °C/100 years (Ganguly *et al.*, 1994), to the temperature range, 500–600 °C, the exsolution of kamacite may not occur by the conventional process, $\gamma \Rightarrow \gamma +$ Ph $\Rightarrow \gamma + \alpha +$ Ph. It is possible that the kamacite regions formed by the decomposition of martensite α_2 which formed

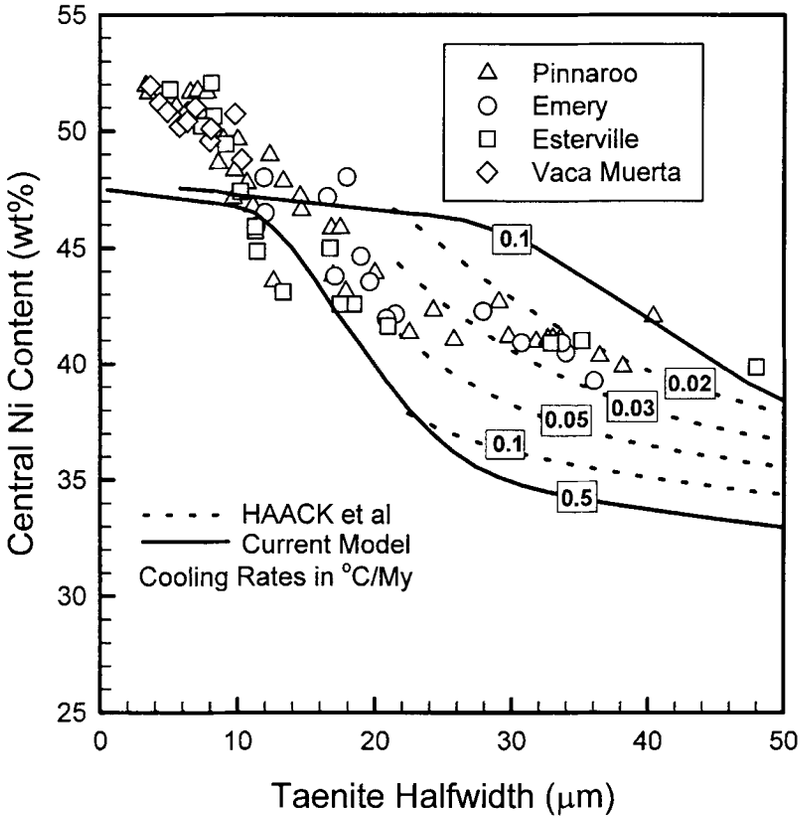

FIG. 11. Central Ni content *vs.* taenite half width plot for the Pinnaroo, Emery, Esterville and Vaca Muerta mesosiderites. The calculated Wood curves from Haack *et al.* (1996) are shown as dashed lines. The calculated Wood curves from the current model (0.1 and 0.5 °C/Ma) are displayed as solid lines.

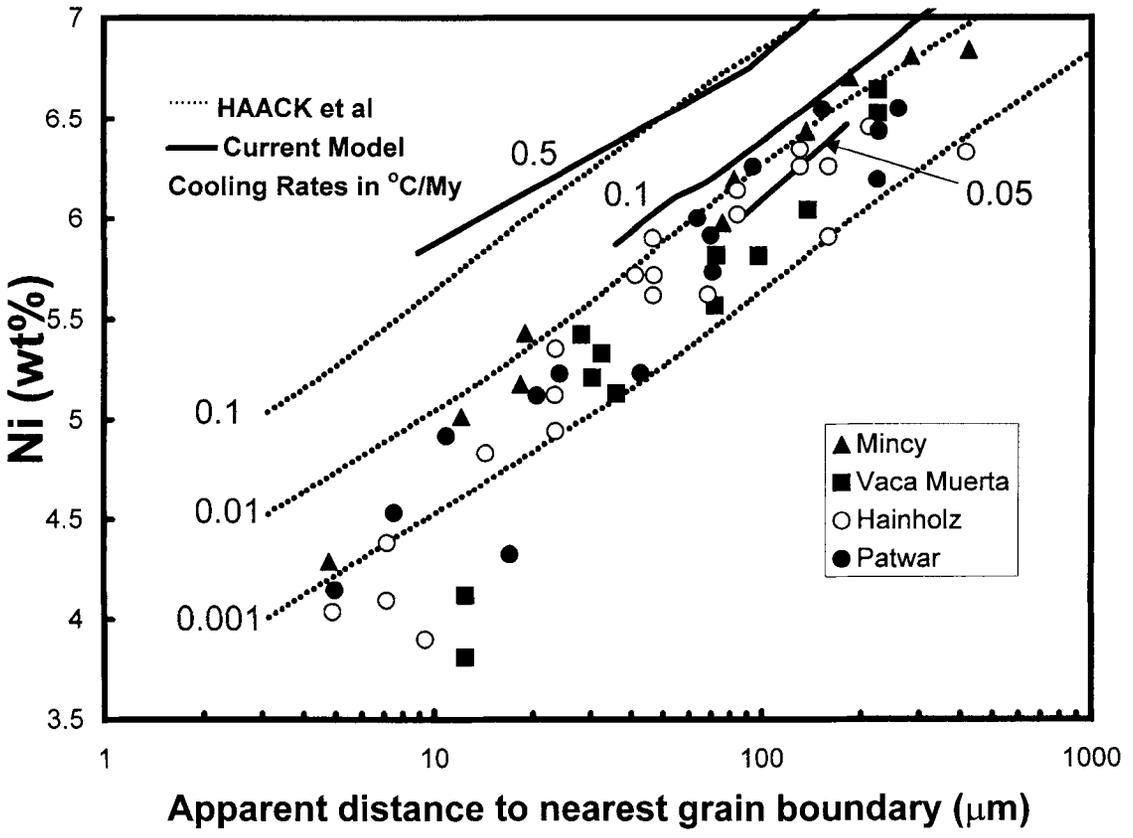

FIG. 12. Central Ni content *vs.* kamacite half width plot for Patwar, Hainholz, Vaca Muerta and Mincy meteorites (data from Powell, 1969). The calculated central Ni content *vs.* kamacite halfwidth curves of Haack *et al.* (1996) are shown as dashed lines and the calculated central Ni content *vs.* kamacite halfwidth curves from the current model are shown as solid lines.

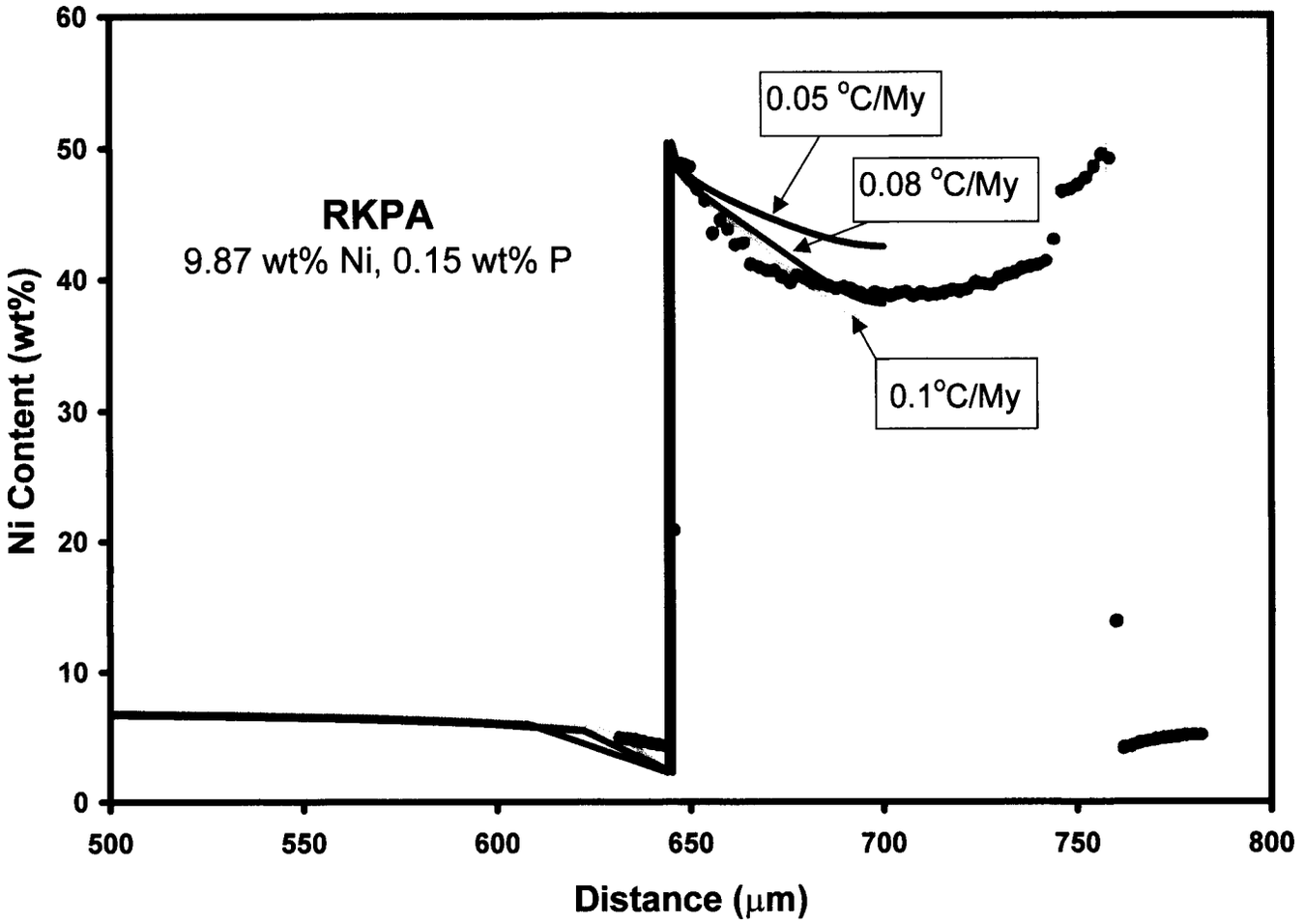

FIG. 13. Ni concentration *vs.* distance across a kamacite-taenite region from an isolated grain in the RKPA79015 mesosiderite as measured using the EPMA (Yang, 1994). The kamacite-taenite Ni profiles, calculated from the current model for 0.05, 0.08 and 0.1 °C/Ma, are superimposed on the measured data.

when the meteorite cooled rapidly below the martensite start temperature. In this transformation sequence, martensite forms and then decomposes at lower temperatures to α kamacite and γ or tetrataenite below 310 °C (see Fig. 1). In this scenario, the growth of tetrataenite is controlled by fast diffusion of Ni through the decomposing α_2, distorted bcc, martensite (Zhang *et al.*, 1993, 1994). This is the same transformation path for the formation of decomposed duplex plessite in iron meteorites (Zhang *et al.*, 1994).

Although we do not have definitive evidence for either explanation of why the current model, $\gamma \Rightarrow \alpha + \gamma$, does not accurately predict the central nickel content of taenite halfwidths smaller than ~10 μm, one can make certain observations using EPMA traces measured across Widmanstätten pattern regions in mesosiderites. Fig. 14 shows an optical picture of a Widmanstätten pattern region in the Vaca Muerta mesosiderite. EPMA data across one of the kamacite bands in the Widmanstätten pattern is shown in Fig. 15. It is important to note that the taenite region surrounding the kamacite plates is almost completely 52 wt% Ni tetrataenite. The tetrataenite is most likely formed by the same process as described for duplex plessite decomposition in iron meteorites (Zhang *et al.*, 1993), $\gamma \Rightarrow \alpha_2 \Rightarrow \alpha + \gamma$. For the mesosiderites on cooling, γ-taenite of ~8 to 12 wt% Ni transforms to martensite, α_2, below the M_S line (Fig. 1). The martensite, α_2, decomposes upon further cooling. Above the monotectoid temperature of 400 °C, martensite α_2 decomposes to $\alpha + \gamma$. Because of the Ni content of the mesosiderite metal and the M_S temperature, the Ni content of the γ phase which forms is no less than about 35 wt% Ni. At lower temperatures, and below the monotectoid temperature, martensite α_2 decomposes to $\alpha + \gamma''$ (Fig. 1). The growth of γ or γ'' precipitates at martensite lath boundaries is due to diffusion control or at lower temperatures to partial interface control (Zhang *et al.*, 1993, 1994). Continued cooling allows γ'' to order forming FeNi, tetrataenite, below 310 °C.

If martensite decomposition controls the microstructure of the metal regions in mesosiderites then the computer simulation model must be changed to reflect the true growth mechanism. A computer simulation model for this

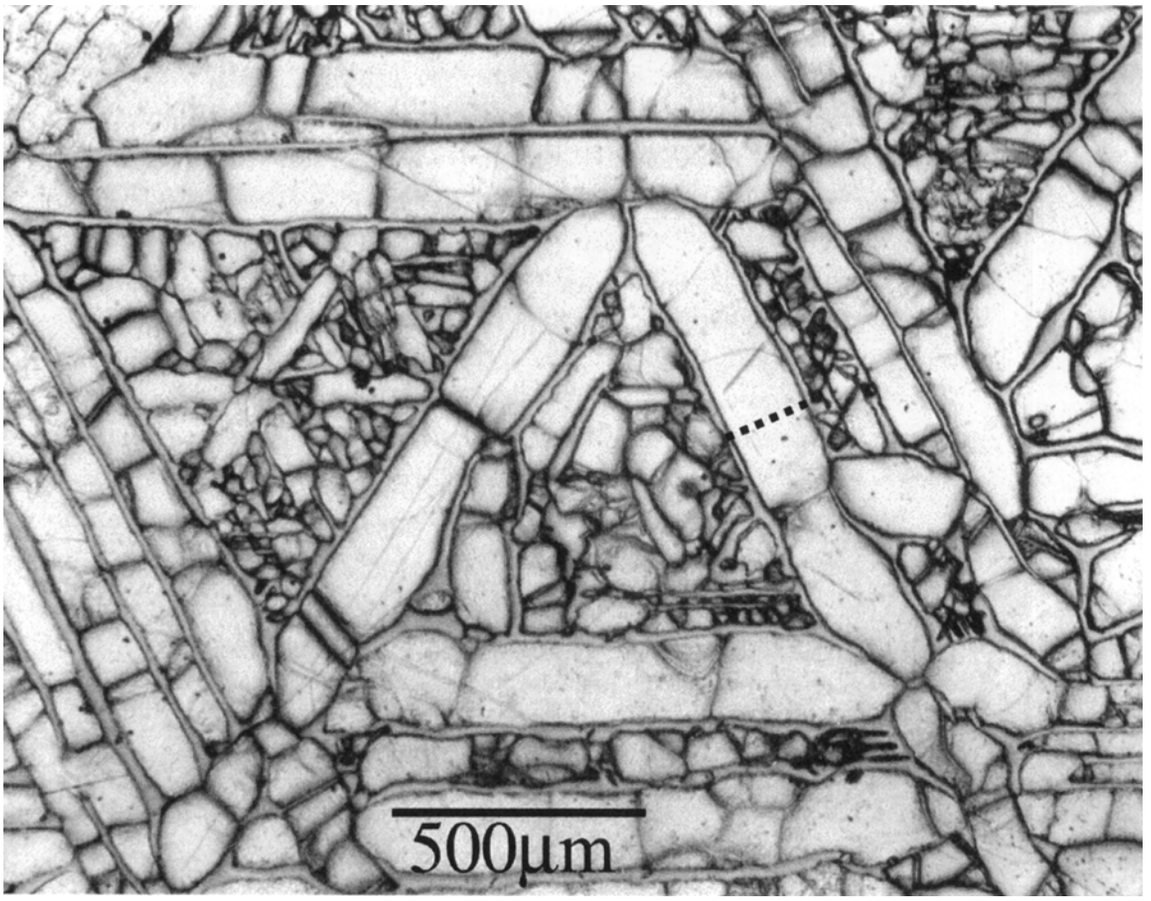

FIG. 14. Optical micrograph of a Widmanstätten pattern region from the Vaca Muerta mesosiderite. The position of the concentration *vs.* distance profile obtained by EPMA is shown by the dashed line.

transformation sequence has not yet been developed. Furthermore, if slow cooling rates begin to occur at temperatures below 400 °C, cooling times for the mesosiderites may no longer be thought of as excessive.

SUMMARY

A major revision of the current Saikumar and Goldstein (1988) cooling rate computer model for kamacite growth has been developed. This revision incorporates a better fit to the $\alpha/(\alpha+\gamma)$ phase boundary and to the $\gamma/(\alpha+\gamma)$ phase boundary particularly below the monotectoid temperature of 400 °C. A reevaluation of the latest diffusivities for the Fe-Ni system as a function of Ni and P content and temperature is made particularly for kamacite diffusivity below the paramagnetic to ferromagnetic transition. It is assumed that the diffusivities in Ni-rich taenite, which forms below 400 °C, can be extrapolated from high temperatures despite the formation of ordered FeNi at lower temperatures.

We have applied the revised simulation model to several iron meteorites and several mesosiderites. For the iron meteorites, the kamacite central Ni content method is quite insensitive to cooling rate variations. For the mesosiderites a cooling rate of 0.2 °C/Ma was obtained using the taenite central Ni content method (Wood method). The measured cooling rate is about 10× higher than the most recent measurements of Haack *et al.* (1996).

The cooling rate curves from the current model do not accurately predict the mesosiderite central nickel content for taenite halfwidths smaller than ~10 μm. There are two possible explanations for this discrepancy: (1) diffusion coefficients in the γ'' phase, which forms as a result of the monotectic below 400 °C, may be inaccurate or (2) the formation of kamacite regions in mesosiderites may not occur by the same transformation sequence as that for the iron meteorites. If the mesosiderites cool rapidly to the temperature range 500–600 °C, martensite, α_2, may form before nucleation of kamacite. The latter explanation may call into question the use of conventional kamacite growth models (metallographic cooling rate methods) to explain the microstructure of the mesosiderites. Kamacite regions in mesosiderites may in fact have formed by the same process as decomposed duplex plessite in iron meteorites

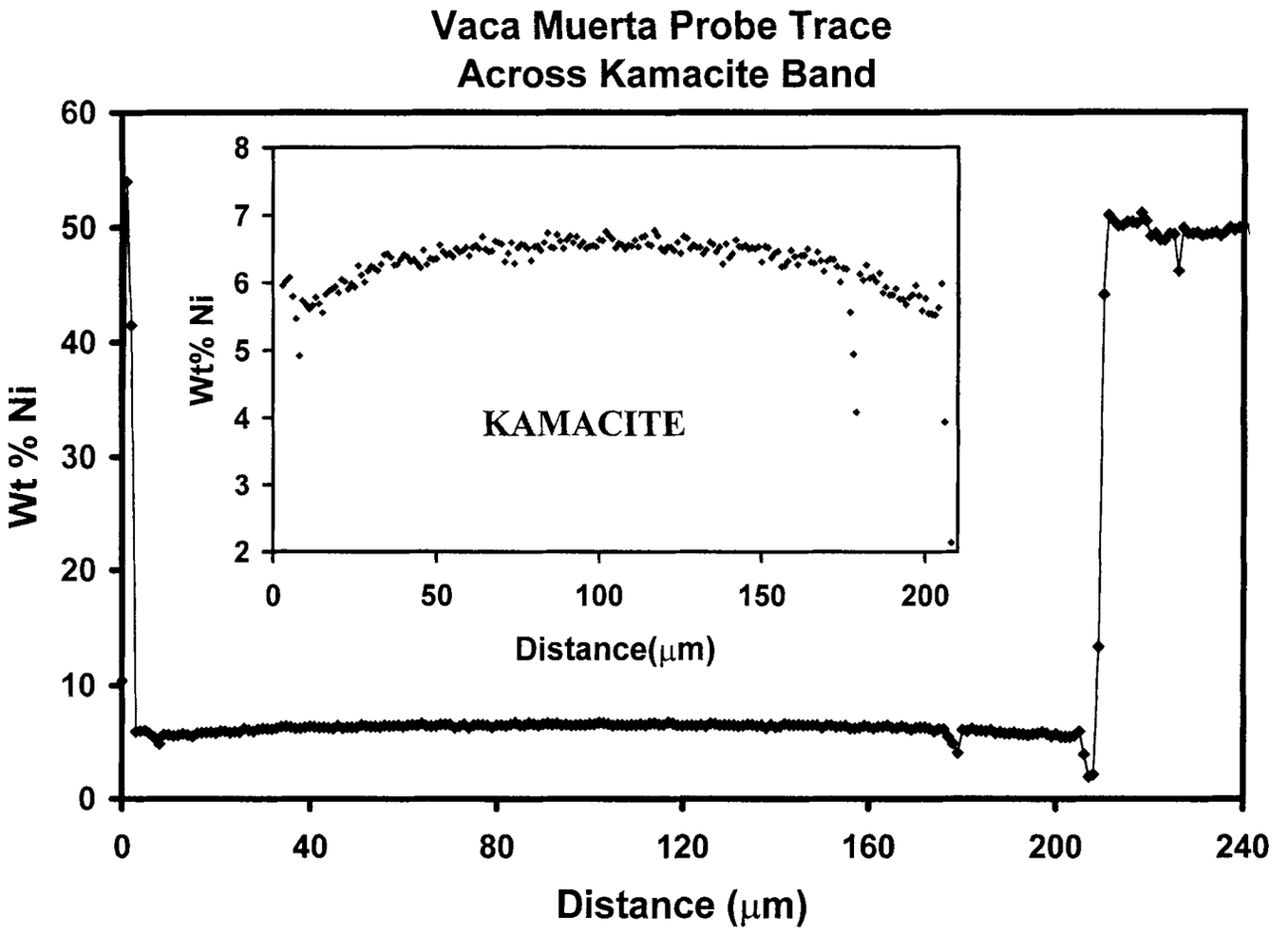

FIG. 15. Ni concentration *vs.* distance across a kamacite-taenite region in the Vaca Muerta mesosiderite (see Fig. 14) as measured using the EPMA. The Ni concentration profile in kamacite is replotted in the inset using a different Ni scale.

(Zhang *et al.*, 1993, 1994). If this process is applicable, then the computer simulation model must be changed to simulate martensite decomposition during cooling.

Acknowledgments–This research was supported by NASA grant #NAG5-4652, J. I. Goldstein, Principal Investigator. The suggestions of Dr. E. R. D. Scott, Univ. Hawaii, Dr. A. E. Rubin, U.C.L.A. and Mr. Rob Reisener, U. Mass Amherst are greatly appreciated. Reviews by J. Ganguly, H. Haack and A. Kracher helped improved the manuscript.

Author Note–The cooling rate computer program for planar kamacite growth is available from the authors upon request. Updates are currently in progress and will be available in the future.

Editorial handling: E. R. D. Scott

REFERENCES

BORG R. J. AND LAI D. Y. Y. (1963) The diffusion of gold, nickel and cobalt in alpha-iron: A study of the effects of ferromagnetism upon diffusion. *Acta Met. Trans.* **11**, 861–866.

BUCHWALD V. F. (1975) *Handbook of Iron Meteorites. Their History, Distribution, Composition and Structure*. Univ. California Press, Berkeley, California, USA. 1418 pp.

CHUANG Y. Y., CHANG Y. A., SCHMID R. AND LIN J. C. (1986) Magnetic contributions to thermodynamic functions of alloys and the phase equilibria of the Fe-Ni System below 1200 K. *Metall. Trans.* **17A**, 1361–1372.

CLARKE R. S. AND GOLDSTEIN J. I. (1978) *Sebreibersite Growth and Its Influence on the Metallography of Coarse Structured Iron Meteorites*. Smithsonian Institution, Washington, D.C., USA. 80 pp.

DEAN D. C. AND GOLDSTEIN J. I. (1986) Determination of interdiffusion coefficients in the Fe-Ni and Fe-Ni-P systems below 900 °C. *Metall. Trans.* **17A**, 1131–1138.

DOAN A. S. AND GOLDSTEIN J. I. (1970) The ternary phase diagram, Fe-Ni-P. *Metall. Trans.* **1**, 1759–1767.

DOAN A. S. AND GOLDSTEIN J. I. (1972) The effect of phosphorus on the formation of the Widmanstätten pattern in iron meteorites. *Geochim. Cosmochim. Acta* **36**, 51–69.

GANGULY J., YANG H. AND GHOSE S. (1994) Thermal history of mesosideritesss: Quantitative constraints from compositional zoning and Fe-Mg ordering in orthopyroxenes. *Geochim. Cosmochim. Acta* **58**, 2711–2723.

GOLDSTEIN J. I. (1965) The formation of the kamacite phase in metallic meteorites. *J. Geophys. Res.* **70**, 6223–6232.

GOLDSTEIN J. I. AND OGILVIE R. E. (1965a) The growth of the Widmanstätten pattern in metallic meteorites. *Geochim. Cosmochim. Acta* **29**, 893–920.

GOLDSTEIN J. I. AND OGILVIE R. E. (1965b) A Re-evaluation of the Iron-rich Portion of the Fe-Ni System. *Trans. Metall. Soc., AIME* **233**, 2083–2087.

GOLDSTEIN J. I. AND SHORT J. M. (1967) The iron meteorites, their thermal history and parent bodies. *Geochim. Cosmochim. Acta* **31**, 1733–1770.

GOLDSTEIN J. I., HANNEMAN R. F. AND OGILVIE R. E. (1965) Diffusion in the Fe-Ni system at 1 Atm and 40 Kbar pressure. *Trans. Metall. Soc., AIME* **233**, 812–820.

HAACK H., SCOTT E. R. D. AND RASMUSSEN K. L. (1996) Thermal and shock history of mesosiderites and their large parent asteroid. *Geochim. Cosmochim. Acta* **60**, 2609–2619.

HASSANZADEH J., RUBIN A. E. AND WASSON J. T. (1990) Compositions of large metal nodules in mesosiderites: Links to iron meteorite group IIIAB and the origin of mesosiderite subgroups. *Geochim. Cosmochim. Acta* **54**, 3197–3208.

HEYWARD T. R. AND GOLDSTEIN J. I. (1973) Ternary Diffusion in the α and γ Phases of the Fe-Ni-P System. *Metall. Trans.* **4**, 2335–2342.

HIRANO K., COHEN M. AND AVERBACH B. L. (1961) Diffusion of nickel into iron. *Acta Met. Trans.* **9**, 440–445.

JAROSEWICH E. (1990) Chemical analyses of meteorites: A compilation of stony iron meteorite analyses. *Meteoritics* **25**, 323–337.

MA L., WILLIAMS D. B. AND GOLDSTEIN J. I. (1998) Determination of the Fe-rich portion of the Fe-Ni-S phase diagram. *J. Phase Equilibria* **19**, 299–309.

MEIBOM A., RASMUSSEN K.L., HAACK H., ULFF-MØLLER F., HORNSHØJ P. AND RUD N. (1994) Carbon in iron meteorites and its importance for metallographic cooling rates (abstract). *Meteoritics* **29**, 501.

MOREN A. F. AND GOLDSTEIN J. I. (1978) Cooling rate variations of group IVA iron meteorites. *Earth Planet. Sci. Lett.* **40**, 151–161.

MURRAY W. D. AND LANDIS F. (1959) Numerical and machine solutions of transient heat-conduction problems involving melting or freezing. Part I–Method of analysis and sample solutions. *Trans. ASME J. Heat Trans.* 106–112.

NARAYAN C. AND GOLDSTEIN J. I. (1984a) Growth of intragranular ferrite in Fe-Ni-P alloys. *Metall. Trans.* **15A**, 876–874.

NARAYAN C. AND GOLDSTEIN J. I. (1984b) Nucleation of intragranular ferrite in Fe-Ni-P alloys. **15A**, 861–866.

NOYE J. (1984) *Computational Techniques for Differential Equations.* Elsevier Science Publ., New York, New York, USA 679 pp.

POWELL B. N. (1969) Petrology and chemistry of mesosiderites—I. Textures and composition of nickel-iron. *Geochim. Cosmochim. Acta* **33**, 789–810.

RASMUSSEN K. L. (1981) The cooling rates of iron meteorites—A new approach. *Icarus* **45**, 564–576.

RASMUSSEN K. L., ULFF-MØLLER F. AND HAACK H. (1995) The thermal evolution of IVA iron meteorites: Evidence from metallographic cooling rates. *Geochim. Cosmochim. Acta* **59**, 3049–3059.

REUTER K. B., WILLIAMS D. B. AND GOLDSTEIN J. I. (1989) Determination of the Fe-Ni phase diagram below 400 °C. *Metall. Trans.* **20A**, 719–725.

ROMIG A. D. AND GOLDSTEIN J. I. (1978) Determination of the Fe-rich portion of the Fe-Ni-C phase diagram. *Metall. Trans.* **9A**, 1599–1609.

ROMIG A. D. AND GOLDSTEIN J. I. (1980) Determination of the Fe-Ni and Fe-Ni-P phase diagrams at low temperatures (700 to 300 °C). *Metall. Trans.* **11A**, 1151–1159.

RUBIN A. E. AND MITTLEFEHLDT D. W. (1993) Evolutionary history of the mesosiderite asteroid: A chronologic and petrologic synthesis. *Icarus* **101**, 201–212.

SAIKUMAR V. AND GOLDSTEIN J. I. (1988) An evaluation of the methods to determine the cooling rates of iron meteorites. *Geochim. Cosmochim. Acta* **52**, 715–726.

WIDGE S. AND GOLDSTEIN J. I. (1977) Redetermination of the Fe-rich portion of the Fe-Ni-Co phase diagram. *Met. Trans.* **8A**, 309–315.

WOOD J. A. (1964) The cooling rates and parent planets of several iron meteorites. *Icarus* **3**, 429–459.

YANG C. W. (1994) Phase decomposition in Fe-Ni system at low temperature. Ph.D. thesis, Lehigh University, Bethlehem, Pennsylvania, USA. 189 pp.

YANG C. W., WILLIAMS D. B. AND GOLDSTEIN J. I. (1996) A revision of the Fe-Ni phase diagram at low temperatures (<400 °C). *J. Phase Equilibria* **17**, 522–531.

YANG C. W., WILLIAMS D. B. AND GOLDSTEIN J. I. (1997) Low-temperature phase decomposition in metal from iron, stony-iron, and stony meteorites. *Geochim. Cosmochim. Acta* **61**, 2943–2956.

ZHANG J., WILLIAMS D. B. AND GOLDSTEIN J. I. (1993) The microstructure and formation of duplex and black plessite in iron meteorites. *Geochim. Cosmochim. Acta* **57**, 3725–3735.

ZHANG J., WILLIAMS D. B. AND GOLDSTEIN J. I. (1994) Decomposition of Fe-Ni martensite: Implications for the low-temperature (<500 °C) Fe-Ni phase diagram. *Met. Mat. Trans.* **25A**, 1627–1637.